The Searchlight Mining District: Linking low sulfidation epithermal mineralization with an underlying granitic pluton using melt and fluid inclusion chemistry

USGS MRERP Award No. 08HQGR0059

Jean Cline and Haroldo Lledo
University of Nevada Las Vegas
4505 Maryland Parkway, Box 454010
Las Vegas, Nevada, USA 89154-4010

Research supported by the U.S. Geological Survey (USGS), Department of the Interior, under USGS award number 08HQGR0059. The views and conclusions contained in this document are those of the authors and should not be interpreted as necessarily representing the official policies, either expressed or implied, of the U.S. Government.

No publications have resulted from work funded by this grant as of 12/31/09

INTRODUCTION

Low sulfidation epithermal systems constitute the second most important source of gold in the United States (George, 2006). Though an accepted model for this type of deposits exists, the relationship between these hydrothermal systems and underlying magma chambers is not well understood. The Searchlight Mining District is a relatively small, but high-grade gold district located in the Colorado River Extensional Corridor (CREC), an area that has undergone a high degree of extension during the Miocene (Anderson, 1971; Anderson et al., 1972; Howard and John, 1987; Anderson et al., 1994; Gans and Bohrson, 1998; Faulds et al., 1999; Faulds et al., 2002a). Low angle extensional faults have tilted the district almost 90 degrees to the west exposing a near complete cross section from upper volcanic rocks on the west, through epithermal veins cutting older volcanic rocks, and into underlying plutonic rocks to the east (Bachl et al., 2001; Faulds et al., 2002b). Based on field relationships and Al-in-hornblende geothermometry Miller et al. (1998) and Bachl et al. (2001) showed that the tilted section represents an almost continuous cross section of about 13 km of paleodepth. This extraordinary exposure provides a rare opportunity to study in detail a low sulfidation epithermal system and to examine its connection with the underlying magma chamber. The fundamental geologic relationships, ore mineralogy and mineral paragenesis, alteration, ore geochemistry have been presented by Callaghan (1939), Shrivastava and Proctor (1962), Longwell et al. (1965), Ludington et al. (2006), and Lledo et al. (2009). This paper builds on earlier work of Lledo et al. (2009) and examines the composition of melt and fluid inclusions using laser ablation induced coupled plasma mass spectrometry (LA-ICP-MS).

Our goals are to understand the processes that link a felsic magma chamber with epithermal mineralization, including chemical evolution of the melt and exsolution of an aqueous fluid. To achieve these goals we (1) determined the composition and trace metal budget of melt inclusions in *pre*-epithermal mineralization melts, (2) determined the composition and trace metal budget of melt inclusions in *post*-epithermal mineralization melts, (3) determined the composition and trace metal budget of *fluid* inclusions in veins containing epithermal Au, and (4) used these data to evaluate the evolving chemistry of the Searchlight pluton and its relationship with aqueous fluids responsible for epithermal precious metal mineralization.

REGIONAL GEOLOGY

Lithostratigraphy

Proterozoic gneiss ranging from 1.8 to 1.5 b.y. (Anderson and Bender, 1989; Young et al., 1989; Young, 1989; Wooden et al., 1988; Wooden and Miller, 1990) forms the basement in the Searchlight Mining District. Notably, Paleozoic and Mesozoic strata are missing due to erosion induced by the Kingman Uplift, a structural feature that extends from the Las Vegas area into western Arizona (Lucchitta, 1966; Young and Brennan, 1974; Bohannon, 1984; Herrington, 2000). The Kingman Uplift formed about 70 Ma and represents the westernmost extent of the Laramide Orogeny in the western United States (Herrington, 2000). As a consequence, thick sections of Miocene volcanic and sedimentary rocks rest directly on Proterozoic metamorphic rocks and Late Cretaceous and Miocene plutonic rocks in the northern CREC (Anderson, 1971, 1977, 1978; Faulds et al., 1990, 1995, 2001; Sherrod and Nielson, 1993). Proterozoic gneiss is

non-conformably overlain by 20 to 18.5 Ma arkosic conglomerate (Faulds et al., 2002a, 2002b) that crops out in the Tip Top Well area, 7.5 km southeast of Searchlight (Fig. 1).

In the rest of the Searchlight District the Proterozoic gneiss is directly overlain by the ~1.5 km thick "Lower intermediate sequence of volcanics of Highland Range" (18.3 to 16.3 Ma) (Faulds et al., 2002a, 2002b), which is included in pre-ore volcanic rocks. These rocks are overlain by a 1 km sequence of rhyolite lavas and tuffs named the "Middle felsic sequence volcanics of the Highland Range" (16.3 to 16.0 Ma) (Faulds et al., 2002a, 2002b), and which are also included in pre-ore volcanic rocks. These volcanic rocks are overlain by megabreccia, conglomerate, trachyandesite to trachydacite and sandstone (16 to 15.2 Ma), the "Upper mafic sequence, volcanics of the Highland Range" (Faulds et al., 2002a and 2002b), included as post-ore volcanics of the Highland Range. These volcano-sedimentary rocks are overlain by the Tuff of Bridge Spring and the Tuff of Mt. Davies, 15.2 ± 0.1 and 15.0 ± 0.1 Ma, respectively (Faulds et al., 2002a and 2002b), that serve as other important stratigraphic markers. The Tuff of Bridge Spring is overlain by post-ore volcano sedimentary rocks (15.0 to 11 Ma) "Middle to late Miocene volcanic and sedimentary rocks" (Faulds et al., 1995; Ruppert and Faulds, 1998; Faulds et al., 2002a and 2002b). All of these volcanic rocks are part of the post-ore assemblage (Figs. 1).

Searchlight Pluton

The Searchlight pluton is a large, ~73 km^2 igneous body that crops out east of Searchlight in the southernmost Eldorado and northern Newberry Mountains. The pluton intrudes Proterozoic gneiss and older Miocene volcanic rocks (Bachl et al., 2001) to the

west, and the late Cretaceous Ireteba pluton to the north and east (Townsend et al., 2000; Kapp et al., 2002) (Fig. 1).

Based on field observations, petrography, and geochemistry Miller et al. (1998) and Bachl et al. (2001) describe the Searchlight pluton as a stratified pluton that can be divided into four main units (Lledo et al., 2009) (Fig 1): upper fine-grained quartz monzonite (~ 2 km thick), middle granite (~ 2 km thick), lower cumulate quartz-monzonite (~ 3 km thick), and lower mafic quartz-monzonite (~2 km thick). Figure 2, although a map view, represents a cross section of the pluton produced by extensional faulting and erosion. East of Searchlight, upper quartz monzonite and overlying volcanic rocks on the southern margin of the pluton have been displaced to the east along low-angle normal faults.

Upper fine-grained quartz monzonite (Bachl et al., 2001) consists of quartz monzonite, quartz monzodiorite, and granite. Miller et al. (2006) obtained ages for upper quartz monzonite of 16.6 ± 0.3 Ma and for a plutonic dike of 16.7 ± 0.3 Ma (Calvin Miller, personal communication) using $^{206}Pb/^{238}U$ in zircon by SHRIMP-RG.

The Middle Unit (Bachl et al., 2001) consists of granite that is more felsic and medium grained than the Upper Unit. This unit includes a late quartzite interpreted as a high silica granite, strongly fractionated, that intruded as dikelets or sills, millimeters to tens of meters in thickness. This leucocratic unit is the latest part of the middle granite unit. The ages of the middle granite range from 16.2 to 15.8 Ma (Dodge et al., 2005, Miller et al., 2006, Miller et al., 2003).

The lower cumulate quartz monzonite consists of coarse-grained quartz monzonite and lesser granite. Miller et al. (2006) obtained an age of 16.1 ± 0.2 Ma for the

lower quartz monzonite near the contact with the middle granite. Miller et al. (1998), Bachl et al. (2001), and Perrault et al. (2005) described the presence of large blocks (1 to 300 m) of Proterozoic gneiss just below the middle-granite/lower-quartz monzonite contact.

The lower mafic quartz monzonite consists of mafic and coarse-grained quartz monzodiorite, locally strongly foliated. Miller et al. (2003), Cates et al. (2003), and Miller et al. (2006) obtained an age for this unit of 16.9 ± 0.2 Ma. This unit contains abundant mafic pods (Miller et al., 1998; Bach et al., 2001; and Perrault et al., 2005). Means et al. (2003) obtained ages for mafic pods of hybrid diorite and coarse-grained gabbro of 16.2 ± 0.2 Ma and 15.9 ± 0.3 Ma, respectively, and Miller et al. (2006) obtained an age for a gabbro pod of 17.7 ± 0.3 Ma.

The significance of these ages is that they indicate a crystallization sequence for the different units of the magma chamber. Although crystallization of the layers overlapped, results suggest that the deepest mafic quartz monzonite layer crystallized earliest and was followed by crystallization of the uppermost quartz monzonite. Crystallization of the quartz monzonite cumulate preceded crystallization of the middle granite unit, which may have been the final unit to crystallize.

Searchlight Mining District, Alteration, Mineralization, and Ore Deposits

The Searchlight Mining District consists of a series of Au-bearing veins with by-product Ag, Cu, Pb, and Zn. The primary metallic minerals are native gold, electrum, chalcopyrite, specular hematite, galena, with local pyrite and sphalerite (Callaghan, 1939; Longwell et al., 1965; Ludington et al., 2006). Surprisingly, pyrite is rare in the entire district (Callaghan, 1939; Longwell et al., 1965; Ludington et al., 2006). These veins are

distributed predominantly in volcanic rocks above the pluton and locally cross-cutting the roof of the Searchlight pluton (Fig. 2).

The distribution of mineralization is notably zoned and former studies (Callaghan, 1939; Longwell et al., 1965; Shrivastava and Proctor, 1962; Ludington, 2006; Castor et al., 2007) highlight the differences in ore, gangue, and alteration mineralogy from north to south. Lledo et al. (2009) showed that the alteration, ore mineralogy, geochemistry, and fluid inclusion microthermometry are also zoned in the east-west direction, which represents a zonation with depth respect to the pluton. The three most important mines of the district include the Quartette Mine (Fig. 2), which was the source of about half of the total production in the district (Callaghan, 1939), the Duplex Mine, and the Blossom Mine (Fig. 2).

METHODS

In order to determine the evolution of the magma and of the fluids that lead to the origin of the Searchlight mining district fluid inclusion petrography and microthermometry, electron microprobe, and laser ablation ICP-MS analyses of fluid and melt inclusions were conducted on samples collected from the main units of the pluton, pre-ore and post-ore volcanic rocks, and from the mineralized veins.

Fluid Inclusion Petrography and Microthermometry

A total of sixteen samples were examined for fluid inclusion studies. Seven samples that contained quartz with visible gold or sulfide minerals and one sample of

translucent sphalerite from productive veins were selected for fluid inclusion microthermometry.

Fluid inclusion petrography was performed at room temperature and inclusion origin, type, and relative age were determined. Fluid inclusion assemblages (FIAs) were identified using criteria of Goldstein and Reynolds (1994). Homogenization and ice melting temperatures were collected with a Linkam THMSG 600 heating and freezing stage mounted on an Olympus BX60 microscope controlled by a Cl93 programmer, LNP cooling pump, and LinkSys software (version 1.83). The system was calibrated using synthetic fluid inclusion standards for temperatures of -56.6 °C, -21.2 °C, -10.7 °C, 0.0 °C, and 374.1 °C. Stage calibration was checked before analysis.

Fluid inclusion data were obtained by first freezing each chip. Ice melting temperatures were determined by monitoring the expansion and contraction of the vapor bubble as temperatures were cycled during heating at subzero temperatures. It was possible to determine the salinity in approximately 80% of the inclusions examined. Homogenization temperatures were determined in 10 °C degree increments during a single heating run on each chip beginning at 50 °C. Chips were held at each heating step for at least 1 minute then cooled 10 °C and inclusions were examined for any phase transitions.

Melt Inclusion Sample Preparation

Compositions of melt inclusions from *pre*-ore and *post*-ore volcanic rocks, and from different units within the pluton were determined by LA-ICP-MS and electron microprobe analysis to investigate the evolution of the melt and to perform a mass

balance calculation. The samples were selected based on field relationships, results of geological mapping, and U/Pb geochronology. Samples were collected from different areas from the Searchlight pluton: upper cumulate quartz monzonite, lower quartz monzonite, the middle granite, high silica granite, and also from pre-ore and post-ore volcanic rocks; the locations of fluid and melt inclusion samples are presented in Figure 3.

Minerals containing melt inclusions were separated using grinding, sieving, heavy liquids, and Franz magnetic separation. The mineral separates were then examined in oil under the microscope and the crystals that contained the largest number of melt inclusions and were least visibly fractured were hand picked. Mineral concentrates were carefully mounted in epoxy and polished until a large number of melt inclusions were exposed at the surface. Melt inclusions were selected for analysis avoiding inclusions near fractures that may have modified inclusion chemistry.

Melt inclusions that had crystallized naturally were heated to rehomogenize them for analysis. This was accomplished by placing a few crystals of a mineral in a small gold crucible placed inside a covered graphite crucible to prevent the sample from oxidizing, and heating in a conventional laboratory oven for 10 minutes. The sample was then quenched and observed under the microscope to check if the melt inclusions homogenized. The procedure was repeated in increments of 50° C until the inclusions were observed to be homogenized. After the approximately homogenization temperature was determined, the remaining crystals were heated in a single step to the homogenization temperature for 10 minutes and then quenched. The required

homogenization temperature for the volcanic rocks was determined to be ~1000° C and for the plutonic rocks was ~950° C.

Electron Microprobe Analysis

Electron microprobe analyses were performed to determine the composition of the melt inclusions and of the mineral hosts. Analyses quantified major oxides including SiO2, Al2O3, MgO, FeO, TiO2, MnO, Cao, Na2O, and K2O; minor oxides including P2O5, SO3, Cr2O3, and V2O3; and also F, Cl and water (interpreted from difference between analysis and 100%). Most analyses of melt inclusions were conducted on homogenized and quenched melt inclusions in order to determine melt volatile contents because LA-ICP-MS cannot reliably analyze H_2O, F, Cl, and S (Pettke et al., 2004). A few analyses were conducted on inclusions that were not heated for comparison. The analyzes were conducted using a JEOL JXA-8900R superprobe at 15 kV accelerating voltage, beam current of 5 nA, and spot size of 3 μm; these conditions avoid potential damage to the melt inclusions, especially regarding volatile and alkali contents. The standards, spectrometers, peak positions, and detection limits are detailed in Table 1.

LA-ICP-MS Analyses

Laser ablation inductively coupled plasma mass spectrometry (LA-ICP-MS) analyses were carried out at Virginia Polytechnic Institute and State University (Blacksburg, USA), using an automated ArF excimer UV (193 nm) MicroLas laser source and analyzed using a quadrupole Agilent 7500ce ICPMS with an octopole reaction cell. The ablated sample was carried by He gas that was then mixed with Ar gas into the

mass spectrometer. The system setup can typically analyze major and trace elements with detection limits < 1 μg/g and with a spatial resolution of ~5 μm. Melt inclusions were analyzed for major oxides Na2O, MgO, Al2O3, SiO2, K2O, CaO, TiO2, MnO, and FeO, and minor and trace elements V, Cr, Co, Ni, Cu, Zn, As, Rb, Sr, Y, Zr, Nb, Mo, Ag, Sn, Sb, Te, Ba, La, Ce, Nd, Sm, Eu, Yb, Jf, W, Au, Hg, Pb, Bi, Th, and U.

The analytical sequence consisted of analyzing background without the laser for 60 seconds followed by analyzing the NIST610 glass standard for 60 seconds with the laser, with a dwell time of 10 μSec; a second NIST610 standard was analyzed and analysis of the unknown samples followed. Two NIST610 standards were analyzed at the end of the run to correct for instrumental drift.

In order to determine the composition of the melt inclusions by electron microprobe and by LA-ICP-MS it was necessary to first determine the composition of the mineral host in order to identify potential interferences by the host in the analyses of the melt inclusions, and to identify systematic variations in the composition of the mineral hosts within the different rock units. The main minerals hosting melt inclusions include clinopyroxene, quartz, sanidine, sphene, zircon, xenotime, and apatite (Fig 4).

The data were reduced using the AMS 1.1.0 software (Scott Mutchler, 2008). Data reduction of melt inclusions exposed on the surface was done directly, while reduction of data for melt inclusions below the section surface was accomplished using a known concentration of one element in the melt inclusion based on 1) microprobe analysis where possible, 2) results of corresponding whole rock analysis, or 3) by assuming a fixed value for the melt inclusion when options 1 and 2 were not available.

The reduced data were evaluated for consistency and analyses that contained common trapped mineral phases such as magnetite, apatite, plagioclase, or orthoclase were discarded. The accepted data were used to document the chemical evolution of the melt, and to determine the relationship of melt evolution to volatile contents that might be involved in precious metal deposition.

RESULTS

Mineralization and Paragenesis

Three hydrothermal events are recognized in different parts of the district. The first event at 17.7 ± 0.1 Ma is characterized by pyrrhotite, bornite, chalcopyrite and biotite and muscovite alteration that may be related to the porphyry copper-type system that was explored by Felmont and Homestake in the 1970s (see Ludington et.al., 2006). The second hydrothermal event is characterized by strong quartz-alunite alteration of rhyolite domes at 17.0 ± 0.2 Ma (Castor et al., 2007); no economic mineralization is associated with this event. The third hydrothermal event corresponds to the formation of the productive precious-metal veins at 16.3 ± 0.1 Ma (Castor et al., 2007) and is described below.

The majority of the veins in the district correspond to the third recognized hydrothermal event and are hosted predominantly in a widespread plagioclase-phyric trachydacite porphyry, to a lesser extent in trachyandesite, trachydacite, and volcanic breccia of the lower intermediate-composition unit of the Volcanics of the Highland Range, and locally in quartz monzonite of the Searchlight pluton.

The hypogene hydrothermal minerals identified by transmitted and reflected light microscopy, energy dispersive spectrometry (EDS), and electron microprobe, from different areas of the district include: specular hematite, galena, chalcopyrite, sphalerite, gold, electrum, pyrite, argentite, rutile, barite, and traces of cassiterite. The supergene minerals include: hematite (replacing chalcopyrite and pyrite), leadhillite, willemite, vanadinite, wulfenite, chrysocolla, Cu-Zn oxide, Cu-Ag-sulfate, iodargyrite (Ag-Cu-I), malachite, native silver, covellite, and larsenite ($PbZnSiO_4$). The mineral paragenesis is summarized below (Table 2).

The earliest hydrothermal mineral found within or near productive veins is specular hematite, which is particularly abundant at the Rambler mine (Fig. 2) where it cements breccias that consist predominantly of trachydacite porphyry, the main host rock in the Searchlight Mining district. A sample from the Quartette mine of trachydacite porphyry is cut by four different generations of veins that exhibit the mineral and vein paragenesis observed over much of the district (Table 2; Fig. 5). The earliest veins consist of quartz with early vein selvedges of specular hematite (V1) (about 2.5 mm width), which also contains minor chalcopyrite disseminated within quartz and locally gold. These veins are truncated by a tectonic or hydrothermal breccia, which is cut by veins of quartz, chalcopyrite, galena, and pyrite (V2). In the Big Casino mine multiple generations of quartz and sulfide veins are present with an early vein consisting of quartz, chalcopyrite, and lesser pyrite, possibly V2. V2 is followed by a massive vein containing galena, sphalerite, chalcopyrite, and pyrite (V3) that exhibits paired exsolution textures consisting of sphalerite-chalcopyrite, sphalerite-pyrite, galena-sphalerite, and galena-chalcopyrite. Synchronous precipitation of sulfides is also suggested by veins of

sphalerite that cut galena, while in other areas galena cuts sphalerite. Vein V3 is cut by quartz with pyrite and chalcopyrite (V4). These veinlets are cut by other quartz veins containing gold, chalcopyrite, and pyrite (V5). A late generation of barren quartz (V6) ~50 μm long crystals, cuts V5 veins. Covellite and native silver, identified with EDS, partly replaced earlier sulfides.

The mineralization has been described as zoned north to south (Callaghan, 1939; Castor et al., 2007) but in addition we observe an east to west zonation that reflects variation from deep (east) to shallow (west). Based on these observations, we classify the deposits in the district based on the original perpendicular distance from the veins to the roof of the pluton and in addition we consider the temporal relationships within the different veins which it was not always possible to determine.

Deep and early veins: The deepest exposures of the veins are located in the eastern part of the district and consist of a locally massive stockwork of specular hematite with minor quartz, chrysocolla, and Pb and Zn oxide minerals filling fractures, with low Au and Ag grades, all hosted in Proterozoic gneiss and in trachydacite porphyry. Based on energy dispersive spectrometry (EDS) the primary ore minerals are chalcopyrite, galena, and sphalerite. A good example of this type of mineralization occurs at the Rambler mine, where veins strike N 70° W and dip 72° S. Similar mineralization occurs at the Boston mine, The New Era mine, Rockefeller mine, and the Dupont Mountain area (Fig. 2) located 16 km northeast of Searchlight that was detached and transported eastward. There are no good age constrains for these vein types other than they post-date trachydacite porphyry dated at 17.1 ± 0.2 Ma and that is cut by base metal-rich veins described below.

These deep veins grade to the west (upward) into intermediate depth and later veins, described below, and to the east (downward) into veins of quartz and epidote with minor Cu and low to nil Au hosted in quartz monzonite.

Intermediate depth and later veins: The intermediate depth veins are characterized by high grades of both base and precious metal. The most important mines belonging to this group are the Quartette, Duplex, and the Big Casino mines (Fig. 2). The hypogene vein mineralogy includes quartz and specular hematite (same as in the earlier veins), but in addition includes abundant chalcopyrite, galena, sphalerite, argentite, rare pyrite, and gold. The supergene mineralogy consists of covellite, native silver, iodargyrite, vanadinite, wulfenite, chrysocolla, malachite, hematite, willemite, larsenite, leadhillite, and cerrusite. The intermediate depth and later veins are zoned toward the north with decreasing base metals and increasing adularia abundance.

Shallow and latest veins: The shallow and latest veins are present in the western part of the district and to the north, they are characterized by an absence of base metals and high grades of Au (up to 1.5 oz/t). Mines that are examples of the shallow veins include the Good Hope, Searchlight Parallel, Searchlight M&M, Blossom, and JET mines. The veins contain quartz, calcite, gold, locally chalcopyrite, pyrite, and abundant adularia, the latter especially in the northern part of the district. These veins are interpreted to represent most of V5.

Fluid Inclusion Petrography and Microthermometry

Fluid inclusion microthermometry was performed on seven quartz samples from different mineralized veins representing different blocks and collected at different distances from the pluton (Fig. 2, Table 3) and on one sphalerite sample that was translucent enough for study (Fig. 6, Table 3). The samples were selected based on the presence of visible gold and/or sulfide minerals. One sample was selected because of the presence of rims and inclusions of specular hematite, the earliest epithermal hydrothermal mineral phases. All observed and evaluated fluid inclusions were two-phase, liquid and vapor inclusions, although there are a few inclusions that contain an unidentified translucent trapped solid phase that did not homogenize upon heating. All analyzed fluid inclusions comprise fluid inclusions assemblages (FIAs) as described in Goldstein and Reynolds (1994). Inclusion origin was determined as follows: primary inclusions were identified by their presence in growth zones and consistent liquid to vapor ratios; primary? inclusions exhibit ambiguous evidence of primary origin such as linear alignment with angles close to 120° but not parallel to the crystal rim or tip; secondary inclusions lie along healed fracture planes; pseudosecondary inclusions lie in healed fractures that terminate within two growth zones; and unknown inclusions have insufficient petrographic evidence to classify them in any of the above categories. Growth zones in quartz were identified using cathodoluminesce or by aligned trapped solid phases. Details about the petrography of each sample are presented in Table 3 and Figure 6; the distribution of microthermometry measurements is presented in Figure 7.

Fluid inclusions from Deep veins, essentially early veins from the southern block, homogenized from 230 to 350° C (n = 455) with most inclusions homogenizing between

280 and 320° C (n = 339). Most salinities ranged from 0.4 to 4.0 wt. % NaCl equivalent (n = 426) and a majority had salinities from 1.0 to 2.8 wt. % NaCl equivalent (n = 358). In intermediate veins from base-metal rich comb quartz, fluid inclusions homogenized between 100 and 350° C (n = 356), with most inclusions homogenizing at 290 to 310° C (n = 187), others between 230 and 270° C (n = 64) and others from 140 to 200° C (n = 62). Salinities ranged between 0 and 2.4 wt. % NaCl equivalent (n = 354), with most inclusions between 0.6 and 1.8 wt. % NaCl equivalent (n = 287). In contrast, fluid inclusions in shallow veins, essentially precious metal-rich trapped approximately 500 meters higher in paleoelevation than deep veins, homogenized from 100 to 300° C (n = 158) with most inclusions homogenizing between 150 and 250° C (n = 129). Salinities ranged from 0 to 1.4 wt. % NaCl equivalent (n =155) and most inclusions had salinities between 0 and 0.2 NaCl equivalent (n = 90). Shallow veins contain coexisting liquid-rich two-phase fluid inclusions and vapor-only inclusions in the same assemblage suggesting boiling. Shallow veins commonly contain plumose textures (Fig. 6K) which are typical of epithermal systems (Sander and Black, 1988) and abundant growth zones containing primary fluid inclusion assemblages; however, most of those primary fluid inclusions had inconsistent liquid to vapor ratios indicating necking down reflecting low temperature trapping, or inclusions were too small to analyze, limited data was collected from these samples.

Geochemistry of Host Minerals by LA-ICP-MS and Electron Microprobe Analyses

Average compositions of mineral hosts determined using LA-ICP-MS and electron probe microanalyses are presented in Tables 4A and 4B, respectively. Apatite was analyzed by electron microprobe (Table 4B) in order to estimate systematic

variations of the volatiles within the pluton; remaining minerals were analyzed using LA-ICP-MS analyses.

The results of apatite analysis show highest chlorine concentrations in upper quartz monzonite (~0.9 wt. %), intermediate to low concentrations in the middle granite unit (0.2 to 0.01 wt. %) and low concentrations in late quartzite within the middle granite unit (0.01 wt. %). The concentrations of chlorine in apatite in pre-ore (0.3 to 0.4 wt. %) and post-ore (0.2 wt. %) volcanic rocks are similar values from the pluton. Sulfur concentrations in apatite (Table 4B) exhibit a more complex pattern as they varied significantly from analysis to analysis in the same sample resulting in high standard deviations.

Clinopyroxenes from pre-ore volcanic rocks contain more Al, Ti, Co, Ni, Cr, Na, Ag, and lesser Mn, Zn, Mo, REE, Pb, than clinopyroxenes from the pluton roof, although they have similar Mg and Fe contents.

Sphene is present in several units of the pluton, especially in the middle granite, and contains up to 0.66 wt. % Y, 0.42 wt % Nb, 372 ppm Sn, 0.49 wt % La, 1.3 wt % Ce, and other light REE. Sphene consistently contained ~0.X ppm and up to 1 ppm Au and 0.56 ppm Ag. Zircon contained ~10 ppm Au, ~ 170 ppm of Ag, 9.5 to 14 ppm Ti, up to 0.15 wt % Y, and up to 1 wt % Hf (Table 4A).

Quartz in rhyolite obsidian contains an average of 87 ppm Ti, permitting calculation of the temperature of quartz crystallization at 787 ± 19° C based on the Ti in quartz geothermometer of Wark and Watson (2006); the calculation assumes an activity of TiO_2 of 0.63, which is a typical value of granitic systems. The presence of sphene and titanomagnetite indicates that the activity of TiO_2 is 0.7 providing a temperature

estimation of 773 ± 19°C. The Ti in zircon geothermometer (Ferry and Watson, 2007) from the middle granite unit, based on 9.5 and 14 ppm Ti, yields temperatures of 775° and 815° C, respectively.

Melt inclusion geochemistry

The compositions of melt inclusions determined using electron probe microanalysis and LA-ICP-MS are presented in Tables 5A and 5B, respectively. Table 6 summarizes melt inclusion results based on microprobe and LA-ICP-MS analyses.

Pre-ore volcanic rocks include strongly altered volcanic rocks that were not analyzed, moderately altered trachydacite porphyry that is the main host of mineralization, and weakly altered trachydacite domes and lavas. Most analyzed pre-ore volcanic rocks contain melt inclusions with low water concentrations, with the exception of the trachydacite porphyry, which contains melt inclusions of high SiO_2-trachydacite composition with up to 6 % water, high base metals and low Au concentrations (Table 6). Melt inclusions in weakly altered pre-ore trachydactie domes and lavas have rhyolite compositions with low water concentrations, and generally low base metals and up to 0.8 ppm of Au. A small rhyolite dome or plug (sample 052406-6) contains silicate melt inclusions and locally sulfide melt inclusions hosted in sanidine and/or plagioclase. The sulfide melt inclusions consist of pyrrhotite and exsolved chalcopyrite based on EDS and elemental maps.

The underlying stratified pluton contains melt inclusions of rhyolite composition with water concentrations ranging from 0.9 to 5.3 wt %, up to 0.21 wt % Cl, and 0.016 to 0.14 wt % SO_3, low base metal concentrations, and high Au concentrations up to 5.8

ppm. In general, higher water concentrations correlate with higher SiO_2 concentrations, and these values increase from upper quartz monzonite to lower cumulate quartz-monzonite to middle granite. Alternatively, base metal concentrations decrease with increasing SiO_2. The post-ore samples contain low volatile concentrations, and relatively high base metals.

Although melt inclusions intersected by fractures were avoided, a few strongly melt inclusions hosted in altered plagioclase were analyzed to evaluate the variations in the chemistry due to alteration. The results show that these melt inclusions were significantly enriched in MgO, FeO, CaO, V, Cu, Zn and depleted in K_2O.

Fluid inclusion geochemistry

Samples from hydrothermal veins were selected to study the composition of the ore fluids. Analysis of fluid inclusions by LA-ICP-MS was performed on samples of known salinity as determined by microthermometry (Lledo et al., 2009). Six quartz samples from different mineralized veins interpreted to reflect different paleodistances above the pluton and one sample of sphalerite were analyzed (Fig. 5). The samples were selected based on the presence of visible gold and/or sulfide minerals. One sample was selected because of the presence of rims and inclusions of specular hematite, the earliest epithermal hydrothermal mineral phase. All the fluid inclusions analyzed are two-phase, liquid and vapor inclusions with homogenization temperatures ranging from 300 to 200° C and salinities ranging from 2 to 0 wt % NaCl equivalent.

The results of the analysis of fluid inclusions by LA-ICP-MS are presented in Table 7. The results confirm that the fluid inclusions are low salinity consistent with the

low salinities determined by ice melting temperature (Lledo et al, 2009). A few analyses suggest that these low salinity fluids contained high concentrations of base metals (Table 7). Results also show minor variations in fluid chemistry with depth. While deeper veins have higher salinities than shallower veins, deep veins contain Na, K, Ca, Mg, Fe, Cu, Zn, and Pb, with almost no precious metals, though sporadic elevated concentrations of Au and Ag are indicated. Shallow veins have very low salinities and the main fluid components are K, Na, Ca, Fe, Cu, Zn, Sb, Sn, Sr, Ba, Ag, and Pb. Au was detected in just one inclusion.

DISCUSSION

Fewer melt inclusion studies have been conducted on plutonic rocks than on volcanic rocks, at least in part because inclusions in plutonic rocks are usually smaller, harder to recognize, and the inclusions crystallized as the melt cooled, producing inclusions containing multiple phases rather than an homogeneous melt (Bodnar and Student, 2006). Nevertheless, studies of these complex inclusions provide the best opportunity to quantify metals and volatiles in addition to silicate components, as demonstrated by previous studies on barren granites in the vicinity of a porphyry molybdenum deposit (Audétat and Pettke, 2003), intrusions related to porphyry systems (Halter et al., 2002a; Student and Bodnar, 2004; Heinrich et al., 2005) and intrusion-related Au (Mustard et al., 2006).

Fluid inclusion microthermometry

Results of fluid inclusion microthermometry indicate a systematic variation in temperature and salinity with the mineral paragenesis: Early and deep veins have higher

Th of 280 to 320° C and salinities of 1.0 to 2.8 wt.% NaCl equivalent; intermediate veins have Th of 290 to 310° C, less have Th of 230 to 270 and 140 to 200° C and salinities of 0.6 to 1.8 wt.% NaCl equivalent, and shallow and late veins have significantly lower Th of 150 to 250° C and salinities of 0.0 to 0.2 wt.% NaCl equivalent. Shallow veins commonly show evidence of boiling which is rare in intermediate veins, and not present in deep veins.

Homogenization temperatures are equivalent to trapping temperatures in boiling systems and represent true trapping temperatures in shallow veins which are approximately 200° C. The corresponding pressure using the equation of state of water (Bodnar & Vityk, 1994) is 15 bars. We can calculate the depth of fluid trapping assuming hydrostatic conditions as ~182 m at those conditions. We can determine the minimum depth of emplacement of the pluton by adding the depth of fluid trapping obtained for the boiling shallow veins (~180 m) to the perpendicular distance from those veins to the contact with the pluton which is 890 m. This calculation yields a minimum depth of pluton emplacement of ~1,072 m. An explanation may be that, since the age of the roof of the Searchlight pluton is older than the age of mineralization, ore fluids were derived from deeper levels, such as the middle granite unit, rather than the top of the pluton. The estimated distance from the shallow veins to the top of the middle granite unit is ~4.5 km.

The analyses of melt inclusions by electron microprobe indicate that melt in the pluton contained higher concentrations of water and chlorine than melts in pre-ore and post-ore volcanic rocks. The concentrations of volatiles in the magma changed with fractional crystallization and chlorine, fluorine, and sulfur decreased as SiO_2 increased. In particular, chlorine is most abundant in upper quartz-monzonite (early pluton unit) and

lower in the middle granite unit (late pluton unit), although results within a single sample vary widely. Chlorine behavior is important as it is a ligand that can complex with and transport base and precious metals from the magma into the fluid phase.

The analysis of melt inclusions by LA-ICP-MS show that Sn, Au, Ag, Mo, and As contents are higher in melt inclusions hosted in plutonic rocks than in melts from pre-ore and post-ore volcanic rocks. The elements Cu, Zn, and Pb have lower concentrations in the plutonic rocks than in the volcanic rocks. High values of Au were consistently detected in melt inclusions hosted in quartz from obsidian rhyolite (sample 050506-28) with no detectable Au in the host, indicating that Au behaved as an incompatible element.

The results of the analysis by LA-ICP-MS of fluid inclusions were somewhat problematic due to the low salinity of the fluid inclusions, their small size (typically < 10 μm), and the long list of elements selected in the analytical routine. These conditions produced results that were commonly below detection limits. Some local high values of Au seem unusual enough that they may correspond to a solid inclusion encountered during the ablation. Analyses of fluid inclusions in sphalerite were mostly unsuccessful as they were rich in Pb, Ag, Ti, Co, and show no resemblance to the composition of fluid inclusions trapped in quartz. No values of Na, K, Ca, were present above detection limits in most analysis of fluid inclusions hosted in sphalerite. Nevertheless, we can conclude that the ore stage fluid inclusions correspond to very dilute fluids that contain primarily base metals and Na and K. K is more abundant than Na in many cases which may be due to the predominant magmatic fluids rather than the overall meteoric water.

REFERENCES

Anderson, R.E., 1971. Thin skin distension in Tertiary rocks of southeastern Nevada. Geological Society of America Bulletin 82, pp. 43-58.

Anderson, R.E., Longwell, C.R., Armstrong, R.L., Marvin, R.F., 1972. Significance of K-Ar ages of Tertiary rocks from the Lake Mead region, Nevada-Arizona. Geological Society of America Bulletin 83, no.2, pp. 273-288.

Anderson, R.E., 1977, Geologic map of the Boulder City 15-minute Quadrangle, Clark County, Nevada: U.S. Geological Survey Geologic Quadrangle Map, GQ-1395.

Anderson, R.E., 1978, Geologic map of the Black Canyon 15-minute Quadrangle, Mohave County, Arizona and Clark County, Nevada: U.S. Geological Survey Geologic Quadrangle Map, GQ-1394, scale 1:62,500.

Anderson, J.L., Bender, E.E., 1989. Nature and origin of Proterozoic A-type granitic magmatism in the southwestern United States of America. Lithos 23, pp. 19-52.

Anderson, R.E., Barnhard, T.P., Snee, L.W., 1994. Roles of plutonism, midcrustal flow, tectonic rafting, and horizontal collapse in shaping the Miocene strain field of the Lake Mead area, Nevada and Arizona. Tectonics 13, no. 6, pp. 1381-1410.

Audétat, A., Pettke, 2003. The magmatic-hydrothermal evolution of two barren graniotes: A melt and fluid inclusion study of the ZRito del Medio and Cañada Pinabete plutons in northern New Mexico (USA). Geochimica et Cosmochimica Acta 67, no.1, pp. 97-121.

Bachl, C.A. Miller, C.F., Miller, J.S., Faulds, J.E., 2001. Construction of a pluton: Evidence from an exposed cross section of the Searchlight pluton, Eldorado Mountains, Nevada. GSA Bulletin 113, no.9, pp. 1213-1228.

Bodnar R.J., Student, J.J., 2006. Melt inclusions in plutonic rocks: Petrography and microthermometry. *In* Melt Inclusions in Plutonic Rocks (J. D. Webster, ed.) Mineralogical Association of Canada, Short Course 36, pp. 1-25.

Bohannon, R.G., 1984, Nonmarine sedimentary rocks of Tertiary age in the Lake Mead region, southeastern Nevada and northwestern Arizona: U.S. Geological Survey Professional Paper 1259, 72 p.

Callaghan, E., 1939. Geology of the Searchlight district, Clark County, Nevada. U.S. Geological Survey Bulletin 906-D, pp. 136-188.

Cates, N.L., Miller, J.S., Miller, C.F., Wooden, J.L., Ericksen, S., and Means, M., 2003, Longevity of plutonic systems: SHRIMP evidence from Aztec Wash and Searchlight plutons, Nevada: Geological Society of America, Abstract with programs, v. 35, no. 4, p. 6.

Dodge, M.C., Miller, J.S., Faulds, J.E., Miller, C.F., 2005. An erupted record from the Miocene Searchlight pluton, Nevada: Geological Society of America Abstracts with Programs. 37, no. 4, pp. 66.

Faulds, J.E., Geissman, J.W., and Mawer, C.K., 1990, Structural development of a major extensional accommodation zone in the Basin and Range province, northwestern Arizona and southern Nevada: In Wernicke, B.P. (Ed.), Basin and Range Extensional Tectonics Near the Latitude of Las Vegas, Nevada: Geological Society of America Memoir, v. 176, p. 37-76.

Faulds, J.E., Geissman, J. W., Shafiqullah, M., 1992, Implications of paleomagnetic data on Miocene extension near a major accommodation zone in the Basin and Range province, northwestern Arizona and southern Nevada. Tectonics 11, no. 2, p. 204-227.

Faulds, J.E., Feuerbach, D.L., Reagan, M.K., Metcalf, R.V., Gans, P., Walker, J.D., 1995. The Mt. Perkins block, northwestern Arizona: An exposed cross section of an evolving, preextensional to synextensional magmatic system. Journal of Geophysical Research 100, no. B8, pp. 15,249-15,266.

Faulds, J.E., Smith, E.I., Gans, P., 1999. Spatial and temporal patterns of magmatism and extension in the northern Colorado River extensional corridor, Nevada and Arizona: A preliminary report. Nevada Petroleum Society Guidebook, pp. 171-183.

Faulds, J.E., Feuerbach, D.L., Miller, C.F., Smith, E.I., 2001. Cenozoic evolution of the northern Colorado River extensional corridor, southern Nevada and northwest Arizona: Pacific Section of the American Association of Petroleum Geologists Publication GB 78 (also Utah Geological Association Publication 30), pp. 239-272.

Faulds, J.E., Olson, E.L., Harlan, S.S., McIntosh, W.C., 2002a. Miocene extension and fault-related folding in the Highland Range, southern Nevada: a three-dimensional perspective. Journal of structural geology 24, pp. 861-886.

Faulds, J.E., Bell, J.W., Olson, E., 2002b. Geologic map of the Nelson SW Quadrangle. Clark County Nevada. Map - Nevada Bureau of Mines and Geology, Report 134, 15pp., 1 sheet.

Ferry, J.M., Watson, E.B., 2007. New thermodynamic models and revised calibrations for the Ti-in-zircon and Zr-inrutile thermometers. Contributions to Mineralogy and Petrology 154, no. 4, pp. 429-437.

Feuerbach, D.L., Smith, E.I., Tangeman, J.A., Walker, J.D., 1993. The role of the mantle during crustal extension: Constraints from geochemistry of volcanic rocks in the Lake Mead area, Nevada and Arizona. Geological Society of America Bulletin 105, pp. 1561-1575.

Feuerbach, D.L., Faulds, J.E., Reagan, M.K., 1999. Interrelations between magmatism and extension in a major accommodation zone, southern Nevada and northwest Arizona. Nevada Petroleum Society Guidebook, pp. 115-138.

Gans, P.B., Landau, B., and Darvall, P., 1994, Ashes ashes, all fall down; caldera forming eruptions and extensional collapse of the Eldorado Mountains, southern Nevada: Geological Society of America, Abstracts with programs, v. 26, no.2, p. 51.

Gans, P.B., Bohrson, W.A., 1998. Suppression of volcanism during rapid extension in the Basin and Range province, United States. Science, 279, pp. 66-68.

George, M.W., 2006. Gold. *In* Mineral Commodity Summaries. U.S. Geological Survey, pp.74-75.

Giggenbach, W.F., 2003, Magma degassing and mineral deposition in hydrothermal systems along convergent plate boundaries: Society of Economic Geologists, Special Publication, v.10, p.1-18.

Glazner, A.F., and Bartley, J.M., 1984, Timing and tectonic setting of Tertiary low-angle normal faulting and associated magmatism in the southwestern United States. Tectonics v. 3, no. 3, p. 385-396.

Glazner, A.F., Nielson, J.E., Howard, K.A., Miller, D.M., 1986. Correlation of the Peach Spring Tuff, a large-volume Miocene ignimbrite sheet in California and Arizona. Geology 14, pp. 840-843.

Halter W.E., Pettke, T., Heinrich, C.A., 2002a. The origin of Cu/Au ratios in porphyry-type deposits. Science 296, pp. 1844-1846.

Halter, W.E., Pettke, T., Heinrich, C.A., Rothen-Rutishauser, B., 2002b. Major to trace element analysis of melt inclusions by laser ablation-ICP-MS; methods of quantification. Chemical Geology 183, pp. 63-86.

Heinrich, C.A., Driesner, T., Landtwing, M.R., Pettke, T., Williams-Jones, A.E., 2005. Vapor transport of ore metals, with a fresh look at the Bingham porphyry. Abstract with Programs Geological Society of America, 37, no. 7, pp. 162 Oct 2005.

Herrington, J.M., 2000, Evolution of the Kingman Arch, Southern Nevada. Thesis (M.S.) University of Nevada Las Vegas.

Hillhouse, J.W., and Wells, R.E., 1991, Magnetic fabric, flow directions, and source area of the lower Miocene Peach Springs Tuff in Arizona, California, and Nevada: Journal of Geophysical Research, v. 96, no.B7, p.12,443-12,460.

Howard, K.A., John, B.E., 1987. Crustal extension along a rooted system of imbricate low-angle faults; Colorado River extensional corridor, California and Arizona. Geological Society of London, Geological Society Special Publications 28, pp. 299-311.

Kapp, J.D., Miller, C.F., and Miller, J.S., 2002, Ireteba Pluton, Eldorado Mountains, Nevada: Late, Deep Source, Peraluminous Magmatism in the Cordilleran Interior: The Journal of Geology, v. 110, p. 649-669.

Lledo, H, Cline, JS, Ludington, S, and Castor, S, 2009, The Searchlight Mining District Nevada USA, linking low sulfidation epithermal mineralization with an underlying granitic pluton: Geology, mineralization, fluid inclusion microthermometry, Pb, S, O, and H isotopes: Manuscript in revision for Economic Geology.

Longwell, C.R., Pampeyan, E.H., Bowyer, Ben., Roberts, R.J., 1965. Geology and mineral deposits of Clark County, Nevada. Nevada Bureau of Mines, Bulletin 62, 218 p.

Lowenstern, J.B., 2003. Melt inclusions come of age. *In:* Melt Inclusions in Volcanic systems (B. De Vivo & R.J. Bodnar, Eds.) Elsevier, Amsterdam (1-21).

Luchita, I., 1966, Cenozoic geology of the upper Lake Mead area adjacent to the Grand Wash Cliffs, Arizona [Ph.D. thesis]: State College, Pennsylvania State University, 218 p.

Ludington, S., Castor, S.B., Faulds, J.E., Flynn, K.S., 2005. The Searchlight district, Nevada: Oxidized but when? Geological Society of America Abstracts with Programs 37, no. 7, pp. 516.

Ludington, S., Castor, S.B., McLaurin, B.T., Flynn, K.S., Faulds, J.E., 2006. Mineral Resource Potential of the Piute-Eldorado Tortoise, Crescent Townsite, and Keyhole Canyon Areas of Critical Environmental Concern, Clark County, Nevada. *In:* Mineral Resource Assessment of Selected Areas in Clark and Nye Counties, Nevada (S. Ludington Ed.) U.S. Geological Survey, Scientific Investigation Report 5197.

McQuarrie, N., and Wernicke, B.P., 2005, An animated tectonic reconstruction of southwestern North America since 36 Ma: Geosphere, v. 1, no. 3, p. 147-172.

Means, M.A., Miller, J.S., Miller, C.F., Cates, N.L., Wooden, J.L., Ericksen, S., 2003. Mafic injection into a nearly frozen magma chamber: failed (?) rejuvenation and local hybridization in the Searchlight pluton, Eldorado Mountains, Nevada (USA). Transactions of the American Geophysical Union 84, pp. F1630-1631.

Miller, C.F., Faulds, J.E., Bachl, C.A., and Ruppert, R., 1998, Searchlight pluton, Eldorado mountains, Nevada; massive pluton emplacement at the onset of extension: Eos, Transactions, American Geophysical Union, v. 79, no. 17, Suppl., pp 342-343.

Miller, J.S., Cates, N.L., Miller, C.F., Wooden, J.L., Means, M.A., and Ericksen, S., 2003, Magmatic construction and duration of solidification of Searchlight pluton,

Eldorado Mountains, Nevada (USA): Eos, Transactions, American Geophysical Union, v. 84, no. 46, Suppl., Abstract V51I-0398.

Miller, C.F., Walker, B.A., Lowery, L.E., Miller, J.S., Bleick, H.A., Faulds, J.E., Furbish, D.J., and Koteas, G.C., 2005, Construction of plutons by horizontal depositional and intrusive sheets: Geological Society of America, Abstracts with programs, v. 37, no.7 p. 130.

Miller, J., Miller, C., Wooden, J., Perrault, D., Hodge, K., Faulds, J., Cates, N., and Means, M., 2006, A 2 million year history of plutonism and volcanism in the Searchlight magma system, Eldorado Mountains, Nevada (USA): Eos, Transactions, American Geophysical Union, v. 87, no. 52, Fall Meeting Suppl., abstract V51E-1714.

Mustard, R, Ulrich, T, Kamenetdky, VS, and Mernagh, T., 2006. Gold and metal enrichment in natural granitic melts during fractional crystallization. Geology, 34, pp 85-88.

Nielson, J.E., Lux, D.R., Dalrymple, G.B., Glazner, A.F., 1990. Age of the Peach Springs Tuff, southeastern California and western Arizona: Journal of Geophysical Research 95, pp. 571-580.

Perrault, D.S., Miller, C.F., Fisher, C.M., Furbish, D.J., Miller, J.S., and Faulds, J.E., 2005, Giant Country rock blocks within the Searchlight Pluton, Southern Nevada: Geological Society of America Abstracts with Programs v. 37, no. 7, p. 309.

Pettke, T., Halter, W.E., Webster, J.D., Aigner-Torres, M., Heinrich, C.A., 2004. Accurate quantification of melt inclusion chemistry by LA-ICP-MS: a comparison with EMP and SIMS and advantages and possible limitations of these methods. Lithos 78, pp. 333-361.

Ruppert, R.F., and Faulds, J.E., 1998, Geologic map of the western half of the Fourth of July Mountain Quadrangle, southern Nevada: Nevada Bureau of Mines and Geology. Open-File Report 98-7, scale 1:24,000.

Sherrod, D., and Nielson, J., 1993, Tertiary stratigraphy of highly extended terranes, California, Arizona, and Nevada: U.S. Geological Survey bulletin 2053.

Shrivastava, J.N., Proctor, P.D., 1962. Trace Element distribution in the Searchlight, Nevada quartz monzonite stock. Economic Geology 57, pp. 1062-1070.

Smith, E.I., Feuerbach, D.L., Naumann, T.R., Mills, J.G., 1990. Mid-Miocene volcanic and plutonic rocks in the Lake Mead area of Nevada and Arizona; Production of intermediate igneous rocks in an extensional environment. *In:* The nature and origin of Cordillera magmatism (Anderson, J.L., ed.): Geological Society of America Memoir 174, pp. 169-194.

Student, J.J., 2002. Silicate melt inclusions in igneous petrogenesis. Unpublished Ph.D. dissertation Virginia Polytechnic Institute and State University, 119 p.

Student, J.J., Bodnar, R.J., 2004. Silicate melt inclusions in porphyry copper deposits: Identification and homogenization behavior. The Canadian Mineralogist 42, pp. 1583-1599.

Townsend, K.J., Miller, C.F., D'Andrea, J.L., Ayers, J.C., Harrison, T.M., and Coath, C.D., 2000, Low temperature replacement of monazite in the Ireteba granite, Southern Nevada: geochronological implications: Chemical Geology, v. 172, p., 95-112.

Thomas, R., Webster, J.D., Davidson, P., 2006. Understanding Pegmatite Formation: The Melt and Fluid Inclusion Approach. *In:* Webster, J.D. (Eds.), Melt Inclusions in Plutonic Rocks. Mineralogical Association of Canada Short Course 36, Montreal, Quebec, pp. 189-210.

Wark, D.A., Watson, E.B., 2006. TitanoQ; a titanium in quartz geothermometer. Contributions to Mineralogy and Petrology 152, no. 6, pp. 743-754.

Webster, J.D., Thomas, R., 2006. Silicate Melt Inclusions in Felsic Plutons: A Synthesis and Review. *In:* Webster, J.D. (Eds.), Melt Inclusions in Plutonic Rocks. Mineralogical Association of Canada Short Course 36, Montreal, Quebec, pp. 165-188.

Williams-Jones, A., Bowell, R.J., and Migdisov, A.A., 2009. Gold in Solution. Elements 5, no. 5, pp. 281-287.

Wooden, J.L., Stacey, J.S., Howard, K.A., Doe, B.R., and Miller, D.M., 1988, Pb isotopic evidence for the formation of Proterozoic crust in the Southwestern United States: In Ernst, W.G. (Ed), Metamorphism and crustal evolution of the Western United States, v. 7, p.68-86.

Wooden, J.L, and Miller, D.M., 1990, Chronologic and isotopic framework for early Proterozoic crustal evolution in the eastern Mojave Desert region, SE California: Journal of Geophysical Research, v. 95, no.B12, p. 20,133-20,146.

Young, R.A., and Brennan, W.J., 1974, Peach Springs Tuff: Its bearing on structural evolution of the Colorado Plateau and development of Cenozoic drainage in Mohave County, Arizona: GSA Bulletin, v. 85, no. 1, p. 83-90.

Young, E.D., Anderson, J.L., Clarke, H.S., and Thomas, W.M., 1989, Petrology of Biotite-Cordierite-Garnet Gneiss of the McCullough Range, Nevada I. Evidence for Proterozoic Low-Pressure Fluid-Absent Granulite Grade Metamorphism in the Southern Cordillera: Journal of Petrology, v. 30, p. 39-60.

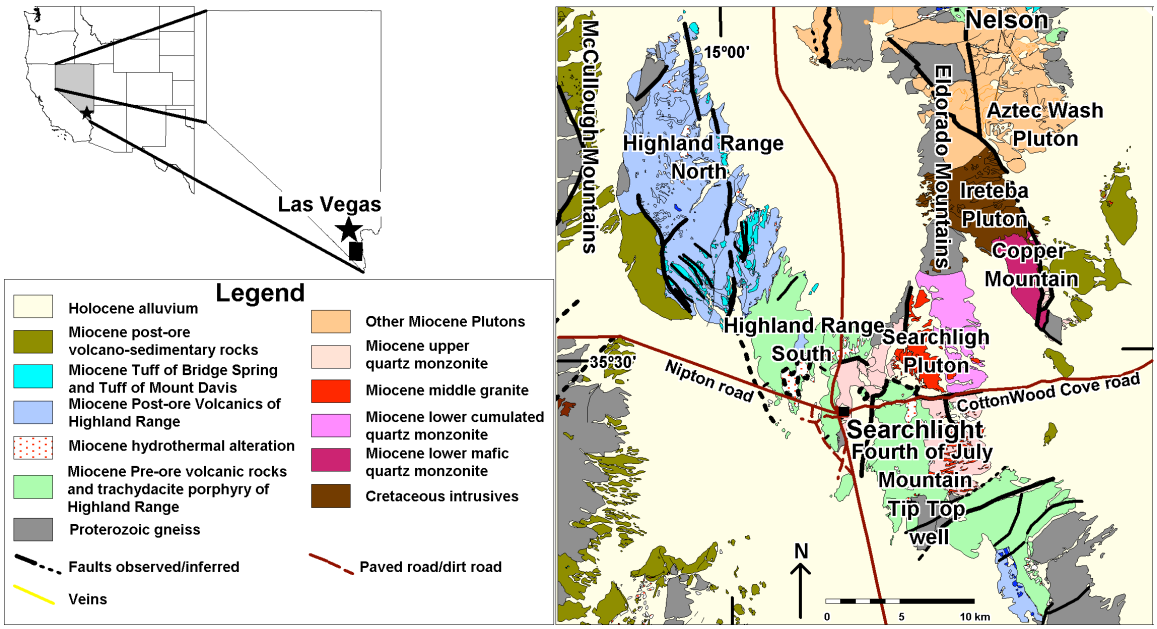

Figure 1: Location map and simplified regional geological map, modified from Bachl et al. (2001) and Faulds et al. (2002a).

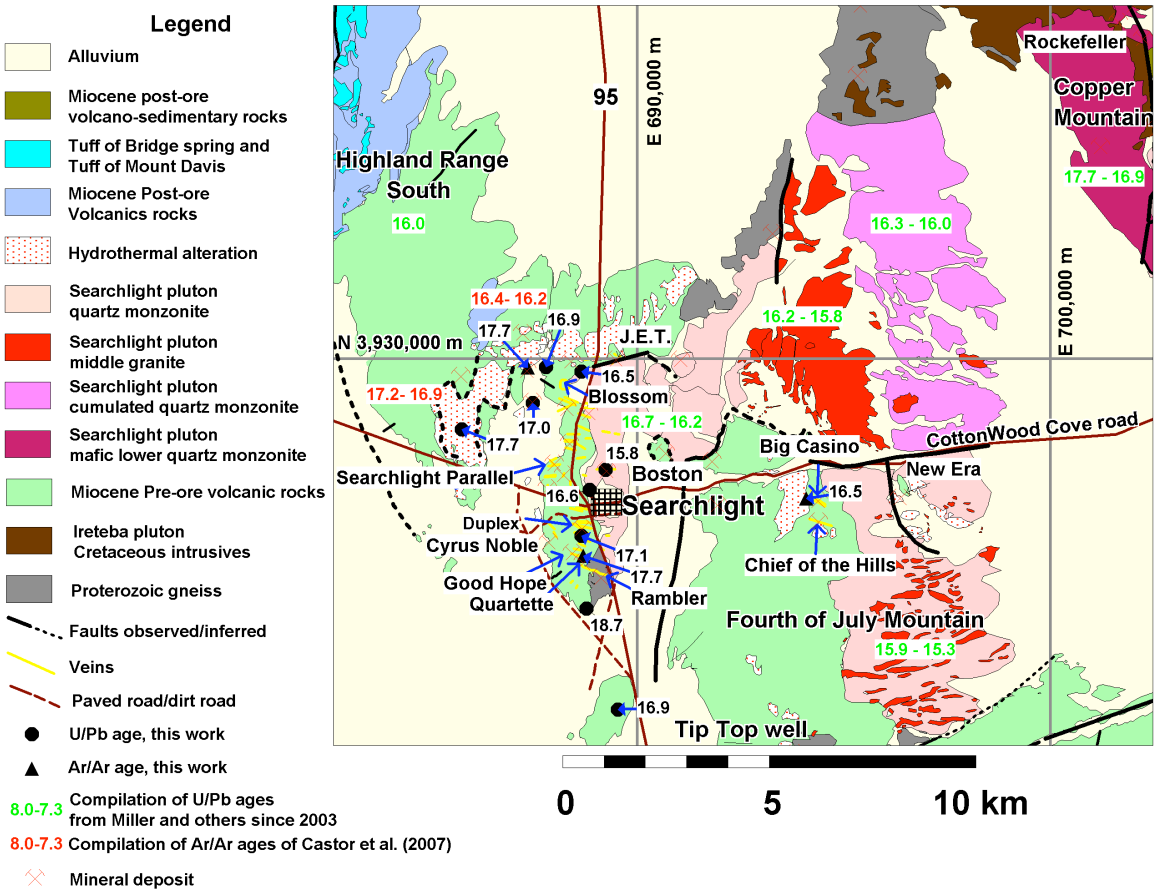

Figure 2. Geologic map of the Searchlight district (modified from Bachl et al., 2001; Faulds et al. 2002b; and Ludington, 2006), showing the location of samples dated in this study using $^{206}Pb/^{238}U$ in zircon and $^{40}Ar/^{39}Ar$ geochronology.

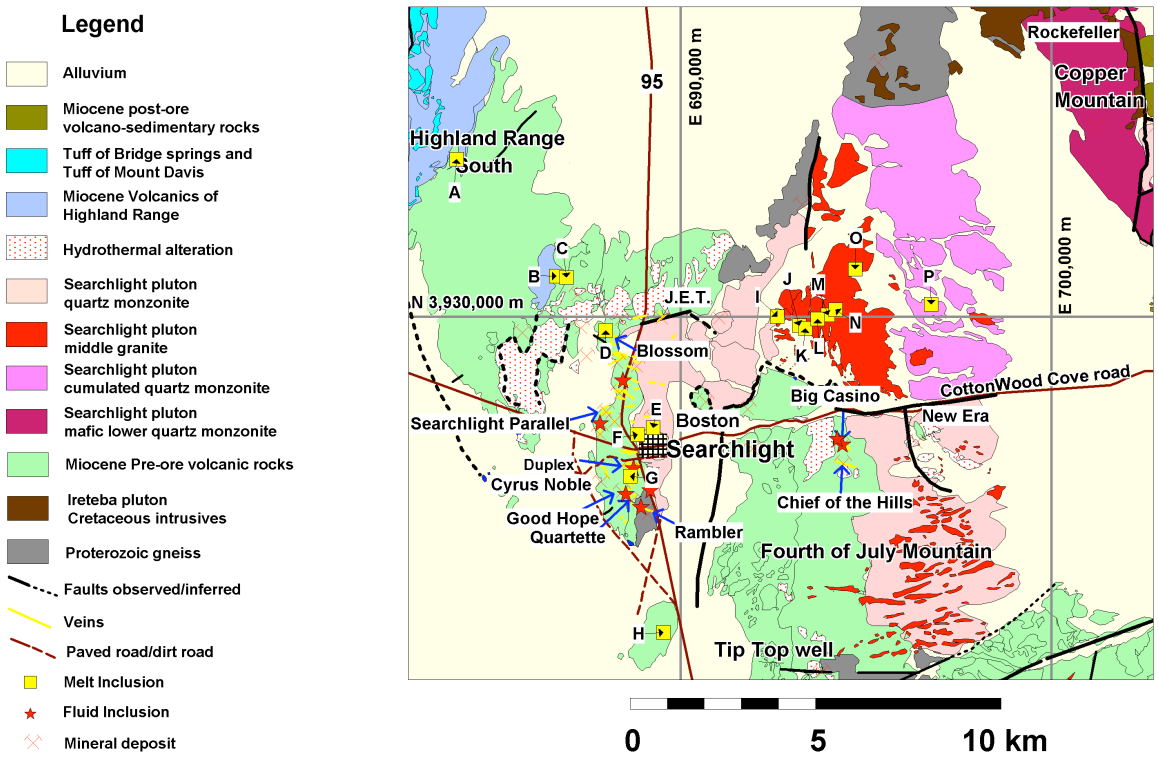

Figure 3. Sample locations for melt inclusion samples. A) 010906-1, B) 050506-26, C) 050506-28, D) 052406-6, E) 042606-14, F) 042606-10, G) 042806-9, H) 011906-4, I) 052606-13, J) 052606-14, K) 052606-11, L) 052606-10, M) 052606-9, N) 052606-5, O) 032206-7, P) 032206-5.

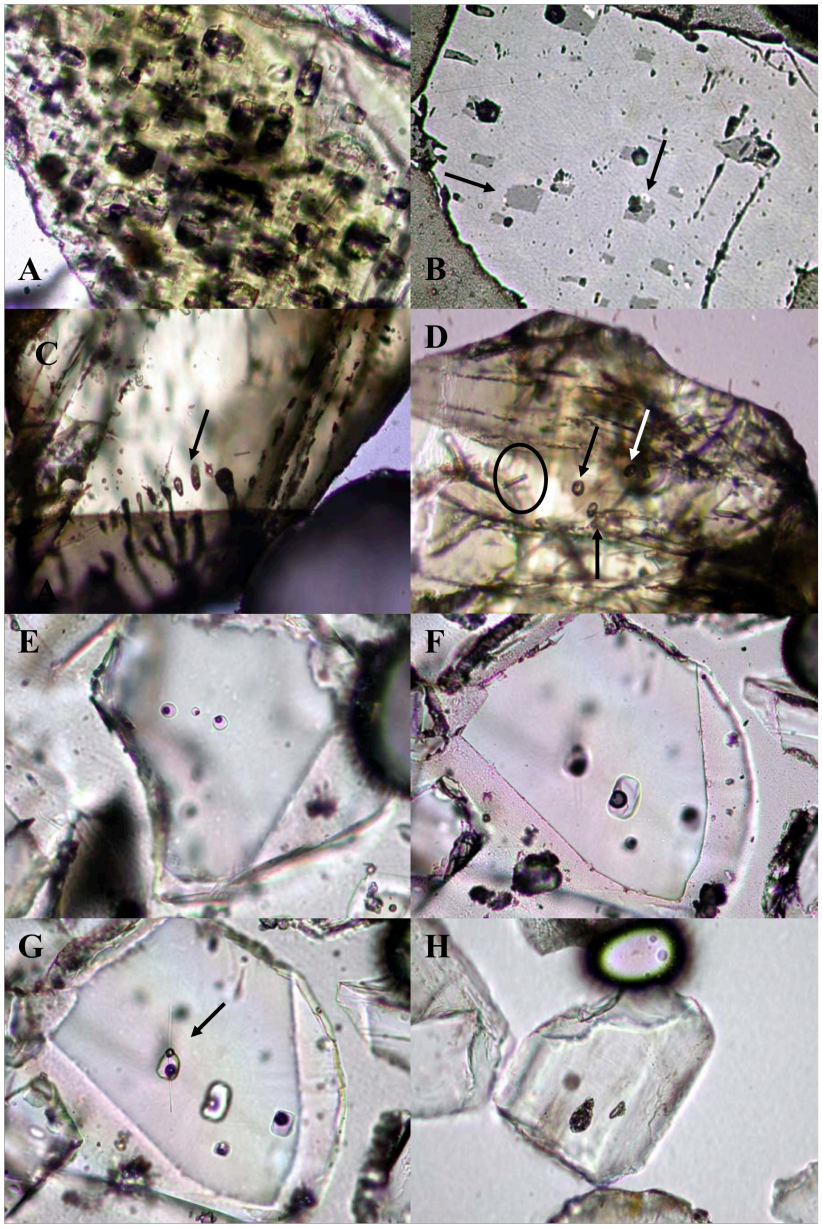

Figure 4. Photomicrographs of unheated melt inclusions from selected samples. The field of view for all photomicrographs is 400 μm. A) clinopyroxene from post-mineral trachyandesite (sample 050506-26) containing multiple irregular to rectangular melt inclusions. B) Same view as in A using reflected light. Some melt inclusions are exposed on the surface and appear darker than the host. The bright rectangles inside some melt inclusions, indicated by the arrows, are

daughter (or trapped) magnetite crystals. C) Sphene crystal from the top of the middle granite unit (052606-11) containing several melt inclusions indicated by the arrow. D) Sphene crystal from the top of the middle granite unit (052606-11) containing 3 melt inclusions indicated by the arrow and several apatite crystals indicated by the oval. E) Quartz from obsidian rhyolite (050506-28) containing 3 melt inclusions in a row. F) Quartz from obsidian rhyolite (050506-28) containing 5 melt inclusions. The melt inclusion at the center of the photomicrograph contains an irregular shaped crystal possibly a trapped sanidine. G) Different view of the same crystal as in F, showing a melt inclusion with a trapped sphene indicated by the arrow and an apatite needle. H) Apatite from a sill of trachydacite porphyry (sample 042806-9) containing a recrystallized melt inclusion.

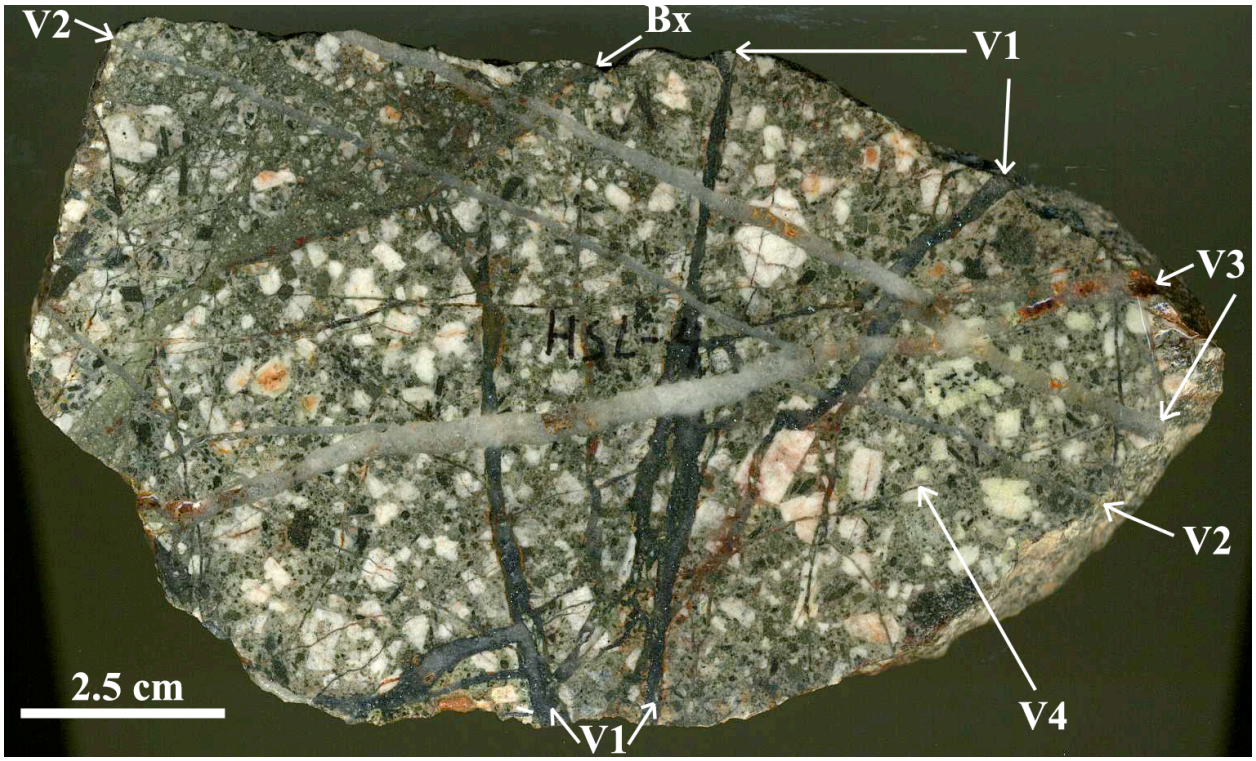

Figure 5. Cross cutting relationships of sample HSL-4 from the Quartette Mine.

Figure 6.

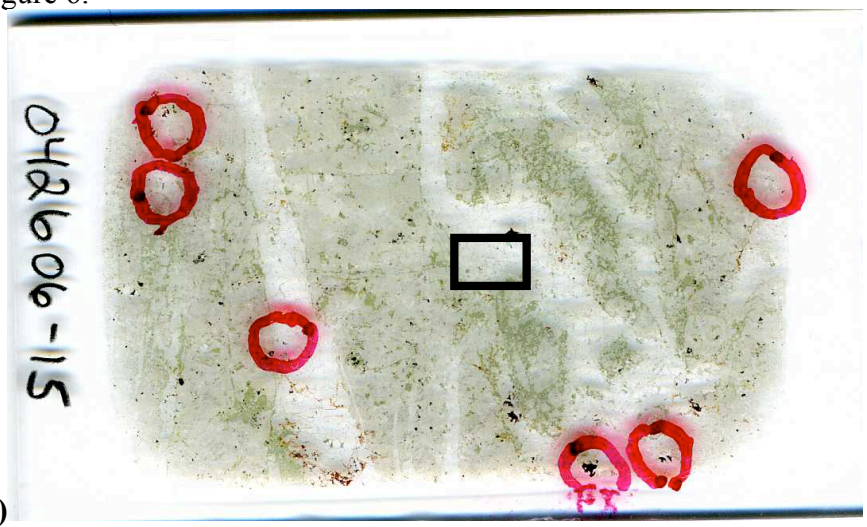

A)

B)

C) 

D) 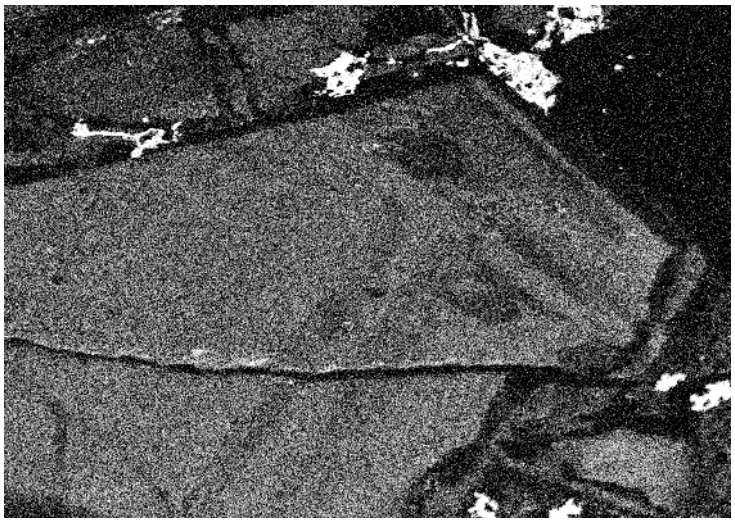

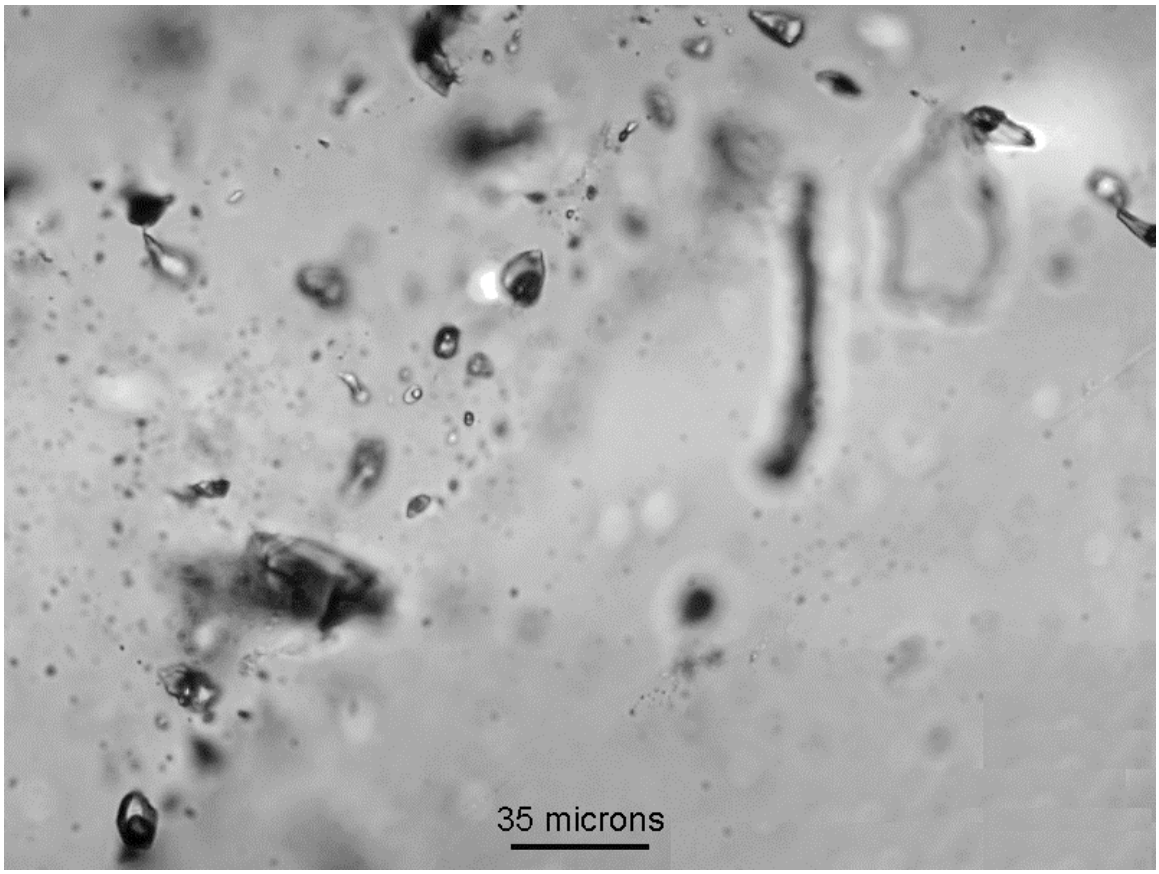

E)

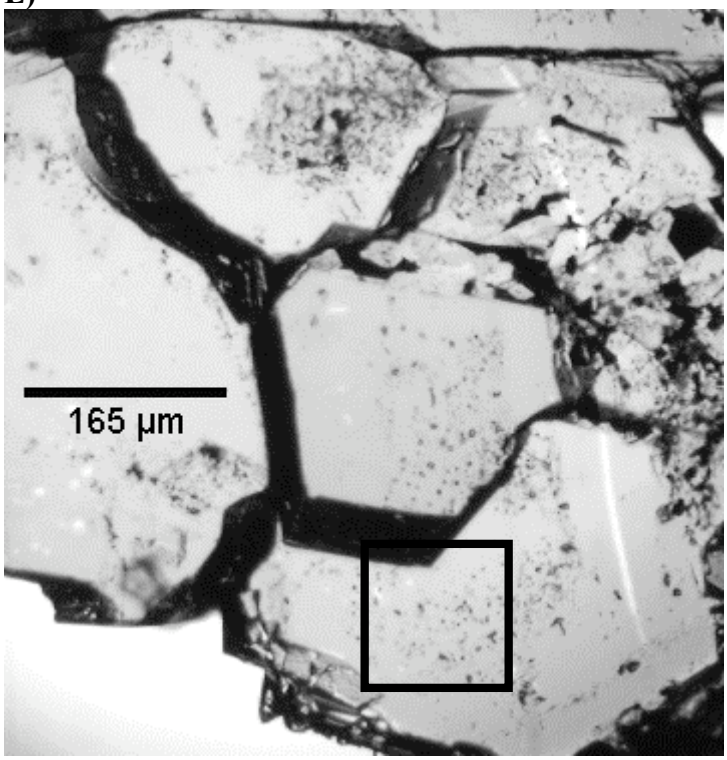

F)

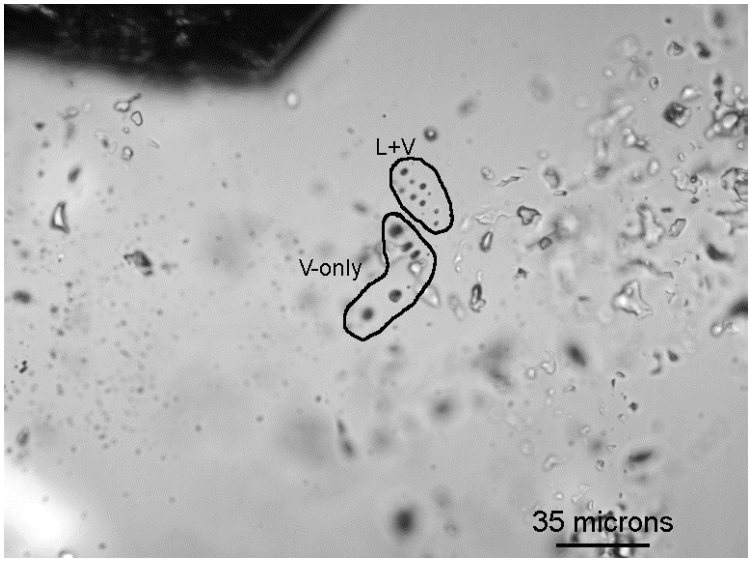

G)

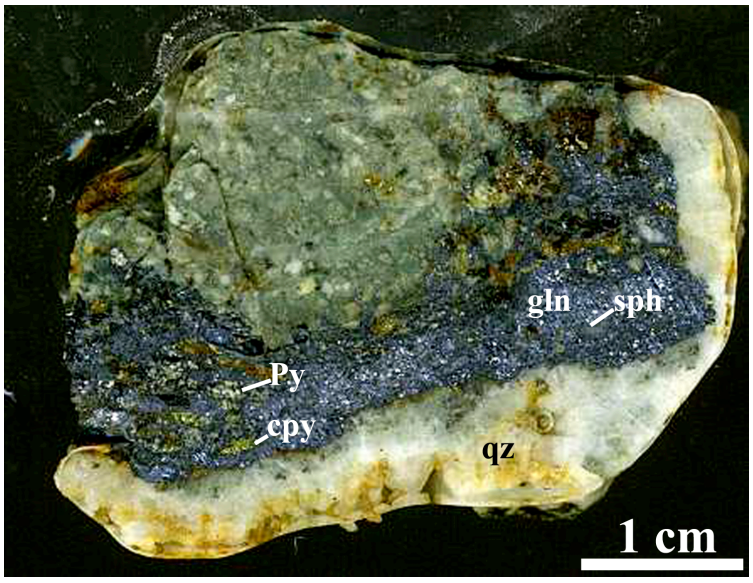

H)

I) 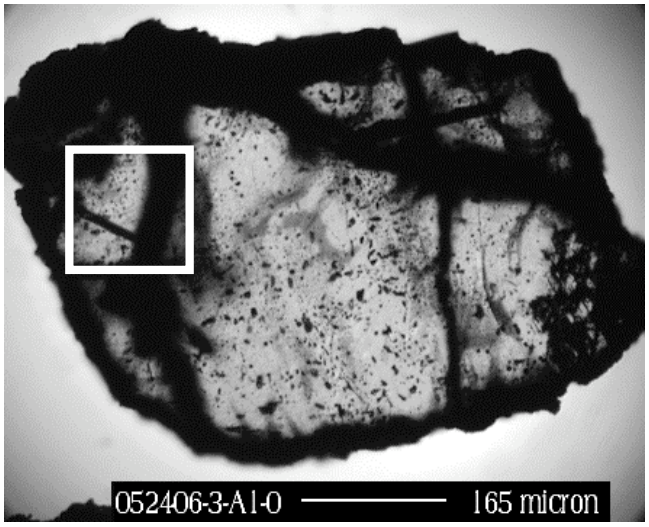

J)

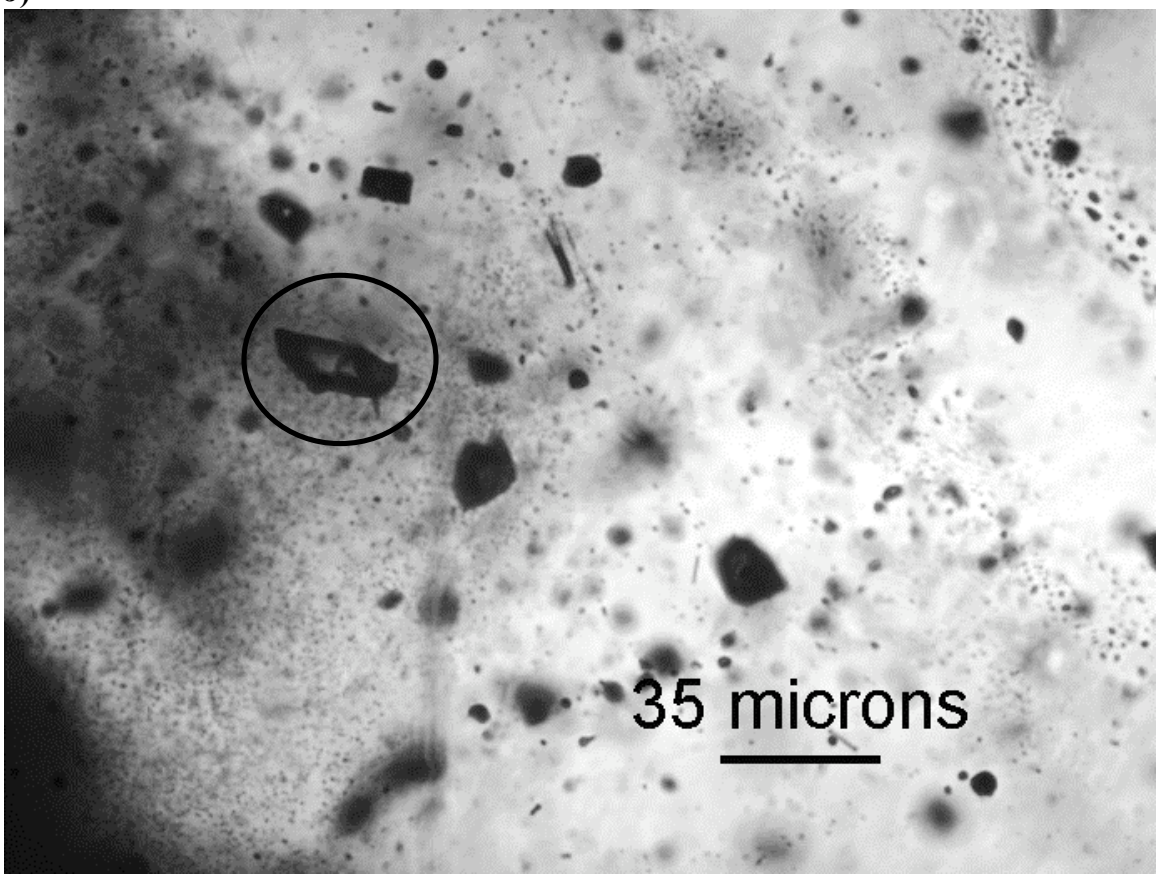

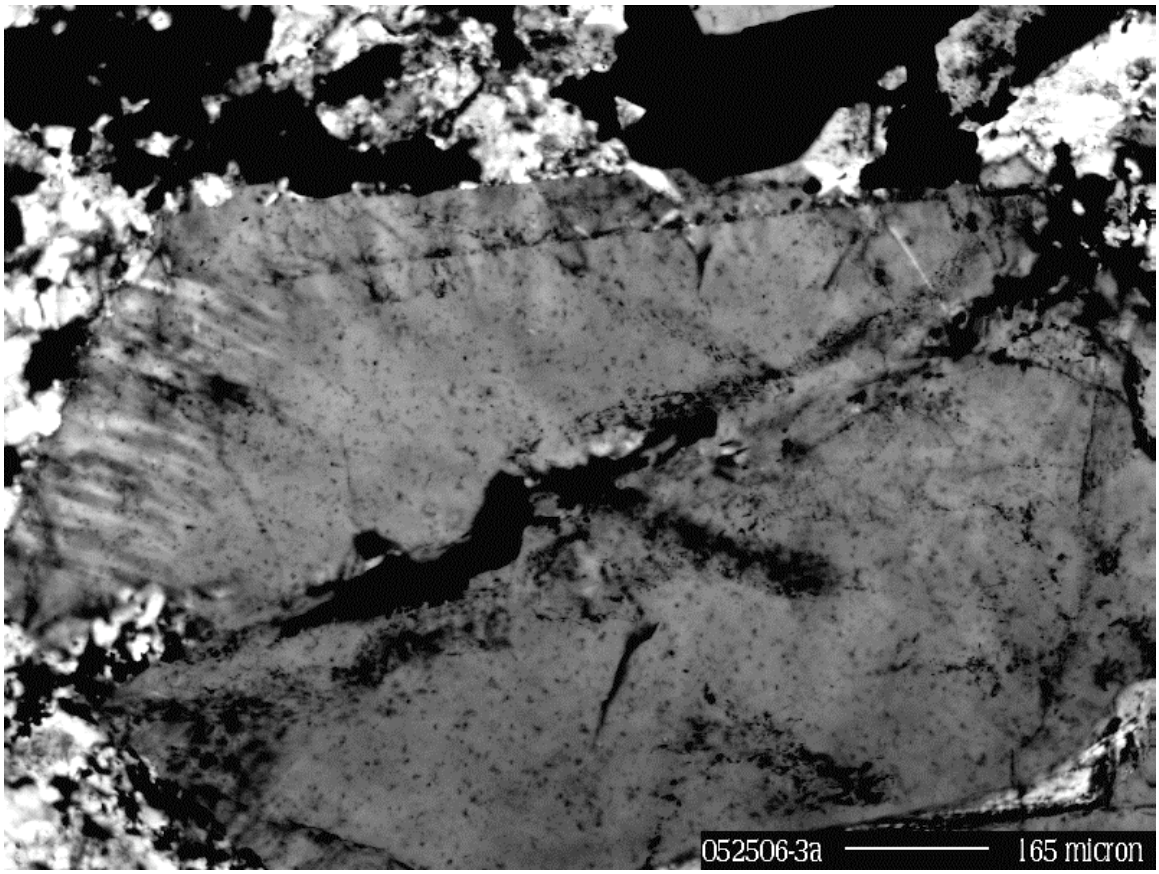

K)

L) 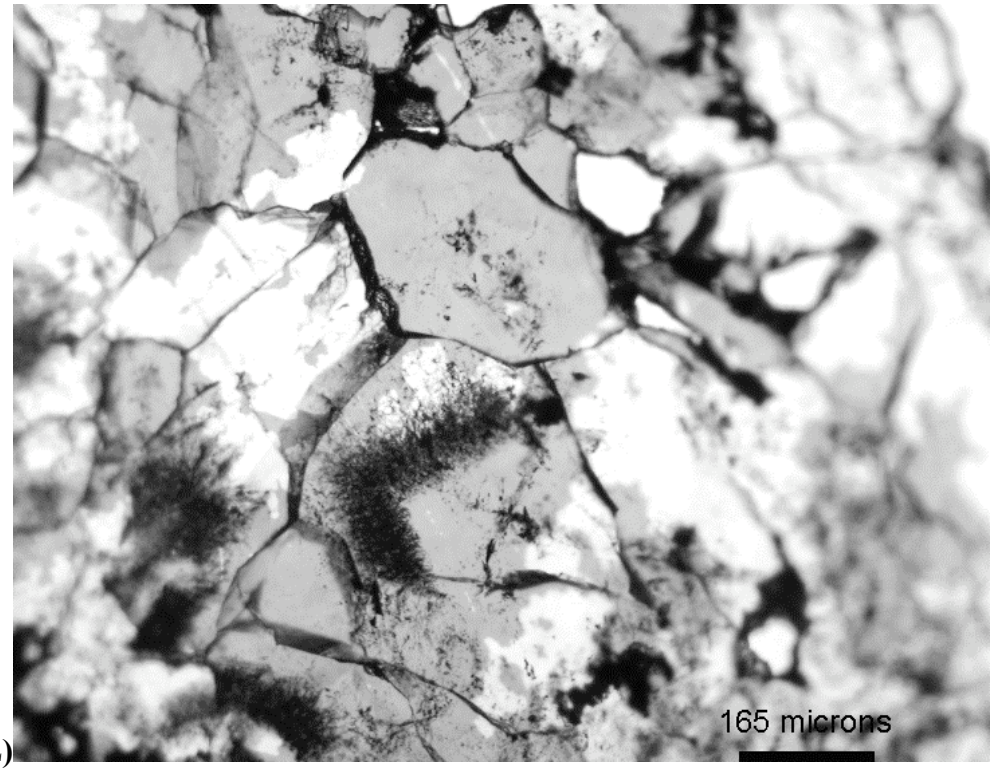

M) 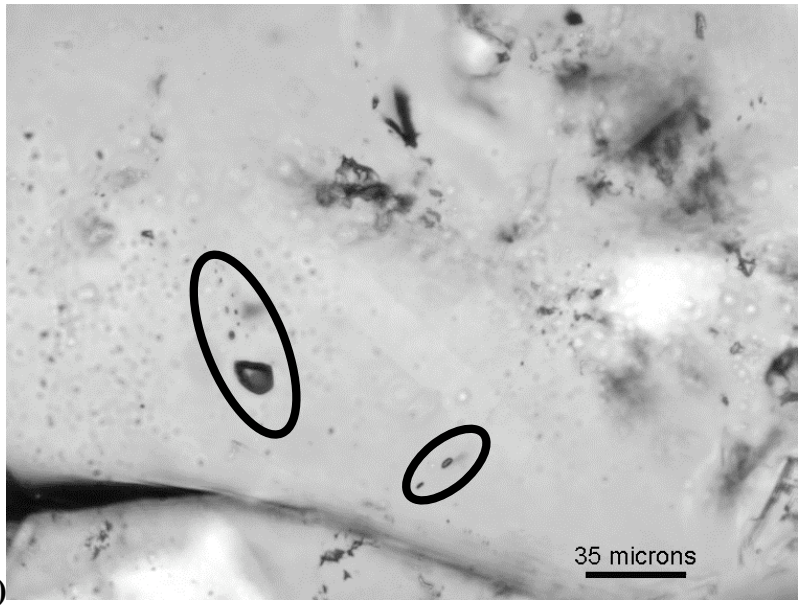

Figure 6. Petrography for fluid inclusion studies. A) Photograph of thin section of sample 042606-15 which corresponds to the pluton roof consisting of quartz-monzonite brecciated and cemented with quartz veins with lesser chlorite, epidote, and K-feldspar. Quartz veins range in thickness from 4 to 10 mm. B) Cathodoluminesce image from square area in (A) shows the strong difference in brightness of magmatic quartz (white), from hydrothermal quartz (gray to black) with distinct growth zones. C) Photograph of

sample HSL-1D consisting of a quartz vein with specular hematite vein selvages cross-cutting trachydacite porphyry and proterozoic gneiss. D) Cathodoluminesce image of sample 050906-5 showing a quartz crystal with growth zones. Black to dark gray is chrysocolla, light gray is quartz with growth zones, bright gray to white is willemite. E) Primary fluid inclusion assemblage from growth zone showed in (D). F) Photomicrograph of quartz from sample 042706-7a-A3 with fluid inclusions along growth zones. G) Coexisting liquid and vapor (L+V) and all-vapor (V-only) FIA from boxed area in (G). H) Sample 052406-3 sulfide rich vein formed by quartz, translucent sphalerite, galena, chalcopyrite and locally pyrite. I) Chip of sphalerite with primary FIA in the square. J) Two-phase fluid inclusions trapped in growth zone. K) Cross polarized photomicrograph of quartz crystal with plumose texture. This texture is characteristic of this sample and of other samples with evidences of boiling. L) Quartz crystals with common growth zones. M) all-vapor fluid inclusion assemblages in secondary planes.

Figure 7.

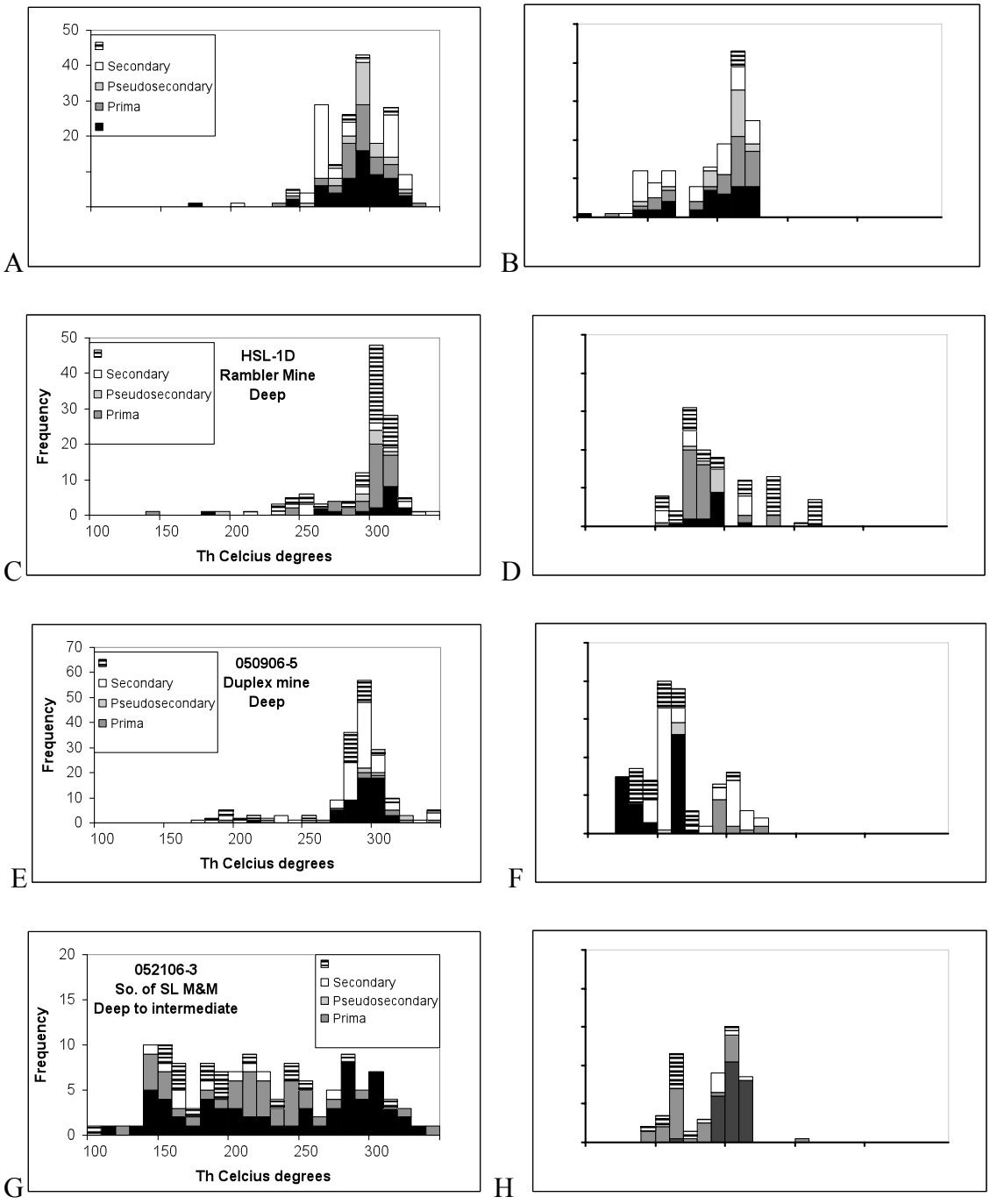
A
B
C
D
E
F
G
H
Secondary
Pseudosecondary
Prima
HSL-1D
Rambler Mine
Deep
Frequency
Th Celcius degrees
050906-5
Duplex mine
Deep
052106-3
So. of SL M&M
Deep to intermediate

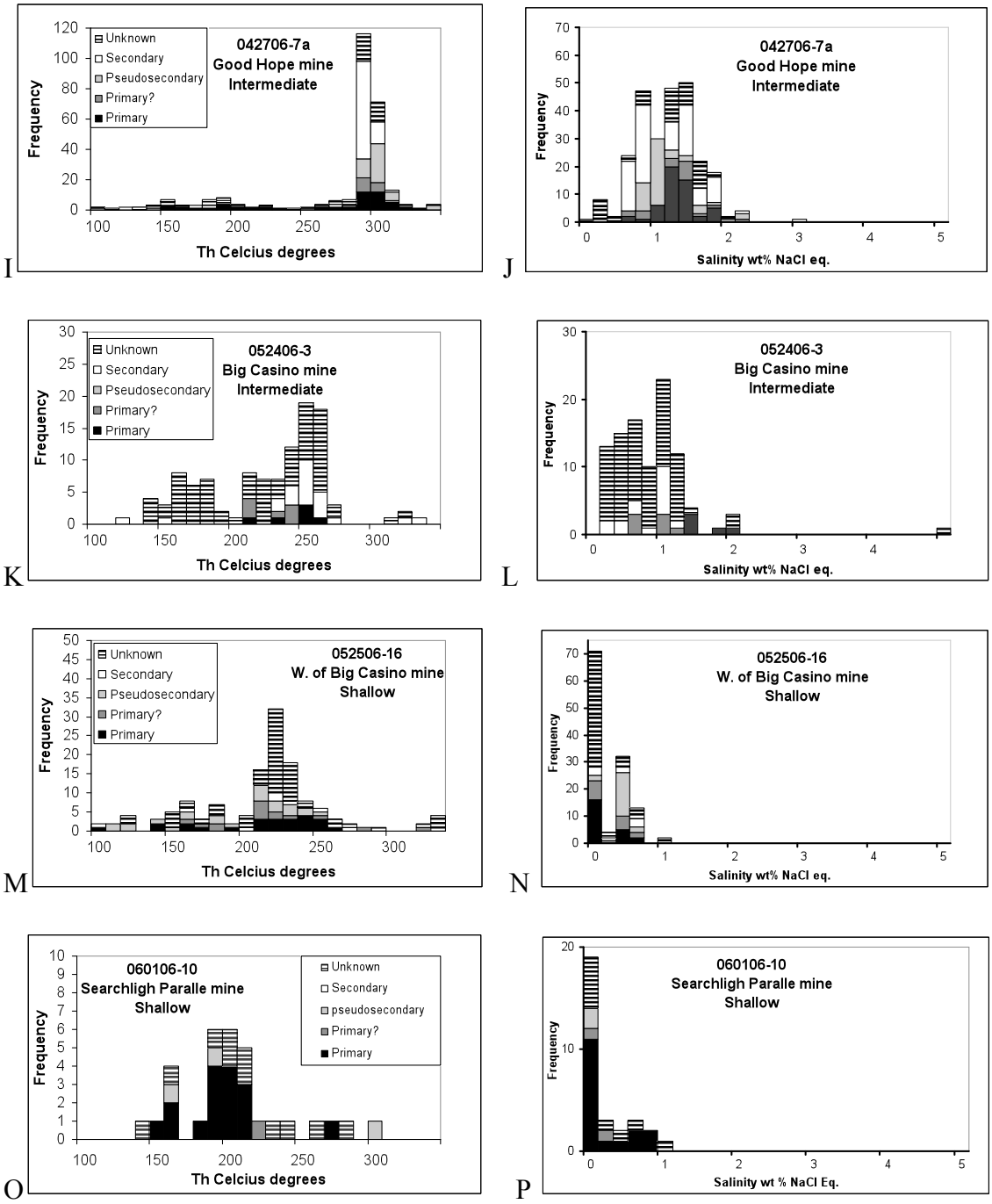

Figure 7. Histograms of homogenization temperatures and salinities determined by fluid inclusion microthermometry.

Table 1. Electron microprobe standards and conditions.

Element	Standard	S	P p	Peak time (seco	Back Counting tim (	Dete Limit (ppm)
S	SMH-Tekit	TAP	7	3	3	264
A	SM	TAP	90	3	3	1
F	SMH-	LI	13	3	3	257
M	SM	TA	10	3	3	1
M	MA -	LI	1	3	2	3
T	SMH-	LI	19	3	3	278
C	SM	PETJ	1	3	3	1
N	SM	TA	12	3	3	1
K	SM	PETJ	1	3	3	1
P	MAC-Apa i	PETJ	19	3	3	320
V	G	LI	1	3	3	276
C	SM	LI	15	6	6	1
C	EM	PETJ	1	1	1	5
F	MAC-Apa i	TA	2	1	1	239
S	M	PETJ	1	1	1	1

Table 2. Paragenesis of observed minerals and cross cutting veins.

Mineral	1	2	3					4
Specular hematite			≡≡(V1)≡ ≡≡	==----				=======
Pyrrhotite	----------							
Bornite	----------							
Chalcopyrite	========			≡≡(V2)≡≡ ≡≡	==(V3)= ====	==(V4)= ==		=======
Pyrite				----(V2)---- ---	----(V3)-- -------	----(V4)-- ------	==(V5)= ==	
Quartz		========		≡≡(V2)≡≡ ≡≡	==(V3)= ====	----(V4)-- ------	≡≡(V5)≡ ≡≡	≡≡(V6)≡≡≡ ======= =
Alunite		========						
Jaraosite-topaz		========						
Adularia							≡≡(V5)≡ ≡≡	
Calcite								≡≡(V6)≡≡≡
Galena				-----	≡≡(V3)≡			
				-	≡≡			
Sphalerite					≡≡(V3)≡ ≡≡			
Acanthite/argentite					----(V3)-- ---			
Gold				---------- ---	≡≡(V3)≡ ≡≡	≡≡(V4)≡ ≡≡≡≡	≡≡(V5)≡ ≡≡	

Table 3. Fluid inclusion microthermometry data for two-phase inclusions.

Sample Location	Utm West	Utm North	Interpreted Vein Depth	Distance to pluton	Geologic context	Vein description
042606-15	689175	3925340	deep	0 m	quartz monzonite from the pluton roof, locally brecciated and cemented with quartz, chlorite, epidote, and K-feldspar and contains several quartz veins ranging in thickness from 4 to 10 mm (Fig. 12A).	The quartz veins exhibit rare specular hematite, chalcopyrite (25 to 10 μm in diameter), galena (5 μm in diameter), traces of cassiterite (< 3 μm in diameter), abundant secondary hematite as pseudomorphs of pyrite and chalcopyrite, and copper oxide minerals.
HSL-1D Rambler mine	688928	3924894	deep	420 m	Sample was selected because it is interpreted to be one of the earliest ore-stage hydrothermal minerals within the district	Quartz veins with selvages of specular hematite (Fig. 12C) and specks of chalcopyrite,
050906-5 Duplex Mine	688725	3925933	deep	340 m		The mineralogy of the vein consists of selvages of specular hematite with the central part of the vein consisting of quartz containing galena, chalcopyrite, sphalerite, willemite, and gold (Fig. 12D, E).
052106-3 So. of SL M&M	688445	3928301	deep to intermediate	450 m		Mineralization consists of a quartz adularia vein containing galena, chalcopyrite, sphalerite, pyrite, and electrum. Some of the quartz has rims with a plumose texture.
042706-7a Good Hope mine	688517	3925247	intermediate	650 m	Mineralization consists of a quartz vein 1 cm wide with visible gold and fragments of altered volcanic rocks, and with a central zone of brown calcite (possibly siderite).	Quartz vein with two size populations without clear cross cutting relationships: a coarse-grained (possibly older) quartz that ranges from 2 mm to 200 μm long, and a fine-grained (possibly younger) quartz of up to 100 μm. The metallic minerals are pyrite, gold, and traces of cassiterite (2 μm in diameter).
052406-3* Big Casino mine	694358	3926571	intermediate	650 m		The vein is complex, formed by different generations of quartz and sulfide minerals. Fluid inclusion microthermometry was performed on sphalerite (Figs. 12H, I, J)
052506-16 W. of Big Casino Mine	694223	3926729	shallow	770 m		Quartz-adularia veins containing electrum.
060106-10 Searchlight Parallel mine	687823	3927143	shallow	890 m		Quartz vein containing electrum, silver-chloride, and argentite (Ag_2S). This sample commonly exhibits growth textures (Fig. 12L) which facilitated the classification of FIAs; however, necking down was very common in these assemblages, which complicated the analysis.

All fluid inclusions are hosted in quartz except sample 052406-3, which is hosted in sphalerite.

Table 3. Fluid inclusion microthermometry data for two-phase inclusions (continued).

Sample Location	Fluid inclusion results
042606-15	Fluid inclusions are predominantly two-phase and liquid-rich. Homogenization temperature ranges from 230 to 340° C (n = 176) with the majority homogenizing from 280 to 320° C (n = 115), salinity of most inclusions ranges from 0.4 to 2.6 wt. % NaCl equivalent (n = 143) but predominantly from 1.6 to 2.6 wt. % NaCl equivalent (n = 108) (Figs. 13A, B). The lowest salinities are associated with FIAs that homogenized at > 320° C.
HSL-1D Rambler mine	Inclusions homogenize from 230 to 350° C (n = 124) with the majority homogenizing between 290 and 320° C (n = 88); most inclusions have a salinity between 1 and 3.4 wt. % NaCl equivalent (n = 115) with the majority having a salinity of 1.0 to 2.0 wt. % NaCl equivalent (n = 80) (Fig. 13C, D). The bases of quartz crystals contain FIAs with homogenization temperatures of 300 to 310° C and salinities of 3.2 to 2.7 wt. % NaCl equivalent, while the middle and tips of quartz crystals contain FIAs with homogenization temperatures of 310° C and salinities of 1.5 wt. % NaCl equivalent.
050906-5 Duplex Mine	Fluid inclusions homogenize between 170 and 350° C (n = 174) with the majority homogenizing between 280 and 310° C (n = 122). The inclusions have a salinity between 0.4 and 2.6 wt. % NaCl equivalent (n = 170) with the majority having a salinity 0.6 to 1.4 wt. % NaCl equivalent (n = 109) (Fig. 13E, F). In this sample it was possible to analyze fluid inclusions trapped in different areas of the same quartz crystal, at the base, in the middle, and near the tip, which was near the center of the vein. Homogenization temperatures in the three areas of the quartz crystal are almost identical at 300° C; however, the salinities progressively decrease from about 2 wt. % NaCl equivalent at the base of the crystal, to ~1.2 wt. % NaCl equivalent in the middle, and ~0.6 wt. % NaCl equivalent at the tip of the quartz crystal.
052106-3 So. of SL M&M	Fluid inclusions homogenize from 90 to 350° C (n = 128) and have salinities between 1.8 and 2.4 wt. % NaCl equivalent (n = 65) and a smaller group between 0.8 and 1.6 wt. % NaCl equivalent (n = 38). Although there is a wide range of homogenization temperatures, they cluster at 180-230, and 270-320° C. Three primary FIAs have a Th of 290° C and a salinity of 2.2 wt. % NaCl equivalent. Secondary and unknown FIAs have a Th of 180 to 260° C and salinities of 2.0 wt. % NaCl equivalent and a few primary FIAs hosted in quartz from a quartz-adularia vein have Th approximately 215° C and salinities of 1.1 wt. % NaCl equivalent.
042706-7a Good Hope mine	Homogenization temperatures range from 100 to 370° C (n = 280) but the majority are between 290 and 310° C (n = 187). Salinities range from 0 to 3.2 wt. % NaCl equivalent (n = 257), with the majority between 0.6 and 2.0 wt. % NaCl equivalent (n = 239) (Fig. 13I, J). One primary FIA contains two-phase fluid inclusions and all-vapor fluid inclusions (Fig. 12F, G) with homogenization temperatures between 170 and 230° C, and salinities that range from 0.7 to 0.9 wt. % NaCl equivalent.
052406-3* Big Casino mine	Homogenization temperatures range from 120 to 360° C (n = 111) with the majority between 240 and 270° C (n = 49). Another group of largely unknown inclusions homogenized between 140 and 190° C (n = 28) (Fig. 13K). Salinities range from 0.2 to 5.9 wt. % NaCl equivalent (n = 98), with the majority between 0.2 and 1.6 wt. % NaCl equivalent (n = 93) (Fig. 13L).
052506-16 W. of Big Casino Mine	Homogenization temperatures range from 50 to 330° C (n = 130) with the majority between 210 and 250° C (n = 74) (Fig. 13M). Salinities range from 0 to 1.4 wt. % NaCl equivalent (n = 125) with the majority between 0 and 0.8 wt. % NaCl equivalent (n = 122) (Fig. 13N). The rims of many quartz crystals have a plumose extinction. This vein contains all-vapor FIAs coexisting with primary? FIAs that homogenize at ~170° C suggesting boiling and a salinity of 0.2 wt. % NaCl equivalent.
060106-10 Searchlight Parallel mine	Homogenization temperatures range from 140 to 310° C (n = 31) with the majority between 190 and 220° C (n = 17) (Fig. 13O). Salinities range between 0 and 1.2 wt. % NaCl equivalent (n = 30) with the majority between 0 and 0.2 wt. % NaCl equivalent (n = 19) (Fig. 13P). Some all-vapor FIAs (Fig. 12M) occur but they were not observed coexisting with two-phase primary FIAs.

All fluid inclusions are hosted in quartz except sample 052406-3, which is hosted in sphalerite.

Table 4A. Average composition of mineral hosts based on LA-ICP-MS

Sample:	Mineral	Comments	Average	Na2O	MgO	Al2O3	SiO2	K2O	CaO	TiO2	V (51)	Cr (52)	MnO
010906-1-1kc	Clinopyroxene	Trachyandesite post-mineral	n=35	0.63	14.99	3.34	51.76	0.04	19.13	0.82	201.60	581.68	0.21
			Stdev	0.11	0.78	0.41	1.29	0.06	1.05	0.09	19.93	331.86	0.02
050506-26-1kC	Clinopyroxene	Trachyandesite post-mineral	n=23	0.56	15.12	2.83	53.49	0.01	18.87	0.58	159.21	1250.17	0.20
			Stdev	0.09	0.71	0.62	0.89	0.01	0.79	0.12	35.71	893.33	0.04
050506-28-1kC	Quartz	Obsidian, syn-ore.	n=17	0.00	BDL	0.02	99.95	0.04	0.00	0.01	BDL	BDL	0.00
			Stdev	0.01	0.00	0.02	0.05	0.04	0.00	0.00	0.00	0.00	0.00
052406-6-1kC	Sanidine	Fresh Trachydacite, premineral (near flow banded)	n=15	3.04	0.00	20.68	63.17	11.65	0.19	0.01	BDL	BDL	0.00
			stdev	0.07	0.00	0.28	0.54	0.26	0.02	0.00	0.00	0.00	0.00
011906-4-1kC	Clinopyroxene	Black trachydacite big hill South of Quartette Pre-ore	n=22	0.48	14.55	1.63	54.07	0.03	19.30	0.38	139.34	120.51	0.34
			Stdev	0.07	1.09	0.46	1.92	0.04	1.44	0.10	20.70	135.15	0.05
042806-9-1kC	Apatite	Dated trachydacite porphyry	n=18	0.22	0.11	0.02	0.57	0.00	96.60	0.00	21.37	5.24	0.11
			stdev	0.03	0.04	0.03	0.11	0.00	0.42	0.00	8.75	0.00	0.03
042806-9-1kC	zircon	Dated trachydacite porphyry	n=3	BDL	BDL	0.01	32.96	BDL	BDL	0.00	BDL	BDL	BDL
			stdev	0.00	0.00	0.01	0.80	0.00	0.00	0.00	0.00	0.00	0.00
042606-10-950C	Clinopyroxene	Dated pluton roof	n=30	0.39	14.35	0.64	54.85	0.02	20.59	0.14	85.11	31.93	0.57
			Stdev	0.03	0.53	0.16	1.10	0.03	1.01	0.04	15.10	33.91	0.10
042606-14-950C	zircon	Reddish pluton roof	n=25	0.00	0.00	0.00	31.45	BDL	0.01	0.00	0.49	BDL	BDL
			Stdev	0.00	0.00	0.00	2.47	0.00	0.02	0.00	0.10	0.00	0.00
042606-14-950C-MI8.txt	sphene	Reddish pluton roof	n=1	0.05	0.01	0.17	34.91	-	26.29	36.32	446.93	-	0.04
052606-13-950C	sphene	Upper monzonite, lower sector near granite	n=25	0.04	0.05	1.20	31.35	0.01	26.31	34.77	705.87	57.56	0.11
			Stdev	0.01	0.08	0.20	1.71	0.03	0.93	1.07	52.58	49.65	0.01
052606-14-950C	sphene	Limit middle granite/upper unit	n=29	0.03	0.03	1.46	31.97	0.00	26.41	34.33	547.88	6.88	0.16
			Stdev	0.01	0.01	0.09	1.99	0.01	1.10	1.02	36.48	1.07	0.01
052606-11-unheated	sphene	Middle granite unit, upper part	n=18	0.03	0.04	1.44	31.59	0.01	26.24	34.77	543.64	7.31	0.16
			stdev	0.01	0.01	0.19	1.17	0.01	1.25	0.92	50.88	1.68	0.02
052606-9-950C	sphene	Coarse grained granite, middle unit	n=36	0.03	0.03	1.51	29.27	0.00	27.44	35.36	562.18	9.90	0.16
			stdev	0.01	0.00	0.11	1.45	0.00	1.37	1.12	51.40	7.07	0.01
032206-7-950C	sphene	Middle granite unit, deep area	n=31	0.05	0.05	1.52	32.78	0.01	25.35	33.05	387.10	9.28	0.27
			stdev	0.01	0.01	0.09	2.31	0.01	1.14	1.23	72.34	8.92	0.04
032206-5-950C	sphene	K-feldspar phyric lower quartz monzonite	n=24	0.02	0.03	1.37	29.94	0.01	26.85	35.86	506.92	13.32	0.17
			Stdev	0.01	0.01	0.17	1.53	0.01	0.98	0.96	41.55	5.37	0.01
052606-5-950C-MI1.txt	zircon	Recrystallized middle unit, very small	n=1	BDL	BDL	BDL	31.44	BDL	BDL	0.00	BDL	BDL	BDL
052606-5-950C	xenotime	Recrystallized middle unit, very small	n=5	0.00	BDL	0.00	2.00	BDL	0.60	0.00	14.01	BDL	0.00
			stdev	0.00	0.00	0.00	0.23	0.00	0.11	0.00	4.57	0.00	0.00
052606-10-950C	zircon	Late quartzite	n=4	BDL	0.00	0.00	29.30	BDL	0.01	0.00	BDL	BDL	BDL
			stdev	0.00	0.00	0.00	2.49	0.00	0.01	0.00	0.00	0.00	0.00
052606-10-950C-MI6.txt	sphene	Late quartzite	n=1	0.05	0.03	1.21	34.68	-	24.63	32.22	659.23	18.89	0.11

Oxides in wt %
Isotope in ppm

Table 4A. Average composition of mineral hosts based on LA-ICP-MS (Continued).

Sample:	FeO	Co (59)	Ni (62)	Cu (63)	Zn (66)	As (75)	Rb (85)	Sr (88)	Y (89)	Zr (90)	Nb (93)	Mo (98)	Ag (107)	Sn (120)	Sb (121)
010906-1-1kc	8.86	51.79	264.44	6.36	88.89	0.79	1.86	119.71	37.19	100.68	0.34	BDL	0.17	1.22	BDL
	0.72	4.88	56.46	2.24	18.97	0.00	2.59	24.36	9.72	24.45	0.29	0.00	0.12	0.26	0.00
050506-26-1kC	8.03	49.47	309.76	9.12	100.34	BDL	0.65	98.23	34.05	81.75	0.31	BDL	0.18	0.98	BDL
	1.34	6.13	48.60	10.55	36.32	0.00	0.13	27.69	16.24	41.90	0.12	0.00	BDL	0.35	0.00
050506-28-1kC	0.00	BDL	BDL	14.23	6.88	BDL	3.17	BDL	BDL	0.61	BDL	BDL	BDL	BDL	BDL
	0.00	0.00	0.00	16.91	9.45	0.00	0.00	0.00	0.00	0.00	0.00	0.00	BDL	0.00	0.00
052406-6-1kC	0.11	BDL	1.33	1.09	3.76	BDL	103.51	729.93	0.13	0.08	BDL	0.23	0.05	0.08	BDL
	0.01	0.00	0.51	0.65	1.65	0.00	4.82	99.56	0.05	0.05	0.00	0.00	BDL	0.00	0.00
011906-4-1kC	9.09	47.40	138.43	4.01	144.26	7.63	2.12	50.25	78.35	77.82	0.38	8.03	BDL	1.18	BDL
	0.63	3.93	35.60	1.36	51.00	0.00	0.00	16.21	13.24	18.45	0.13	0.00	BDL	0.38	0.00
042806-9-1kC	0.12	BDL	12.84	6.94	BDL	39.18	BDL	1408.07	956.61	3.28	BDL	0.66	BDL	BDL	BDL
	0.03	0.00	0.00	7.65	0.00	14.18	0.00	597.95	202.35	0.66	0.00	0.00	BDL	0.00	0.00
042806-9-1kC	0.00	BDL	BDL	3.80	BDL	BDL	BDL	0.17	610.69	486782.35	23.94	BDL	173.03	BDL	BDL
	0.00	0.00	0.00	0.00	0.00	0.00	0.00	0.06	369.57	5265.89	2.44	0.00	6.86	0.00	0.00
042606-10-950C	8.37	37.03	72.93	5.65	155.10	2.20	5.76	16.82	127.19	25.92	0.28	0.73	BDL	1.35	BDL
	0.62	4.75	20.80	5.83	12.42	0.00	4.85	5.94	27.41	13.60	0.12	0.26	0.00	0.41	0.00
042606-14-950C	0.00	BDL	BDL	BDL	BDL	BDL	BDL	0.17	648.83	498452.43	20.46	BDL	170.12	BDL	BDL
	0.00	0.00	0.00	0.00	0.00	0.00	0.00	0.10	261.53	17955.62	1.46	0.00	10.72	0.00	0.00
042606-14-950C-MI8.txt	1.78	BDL	59.40	8.54	BDL	21.39	BDL	255.42	13.92	BDL	861.22	95.29	BDL	371.84	24.22
052606-13-950C	2.03	1.08	57.07	5.48	9.80	44.60	1.27	9.86	3178.09	1057.55	4264.39	135.45	0.56	259.79	2.01
	0.28	0.68	7.61	1.33	1.69	11.45	1.09	7.58	1334.35	707.50	2216.75	0.00	0.31	65.19	2.11
052606-14-950C	1.90	0.43	63.18	5.41	10.16	41.80	0.62	35.79	3533.46	755.45	1832.67	39.41	0.38	151.43	BDL
	0.19	0.00	7.99	0.96	2.94	14.67	0.37	6.89	1512.25	94.25	246.29	5.35	0.13	27.31	0.00
052606-11-unheated	1.94	BDL	53.35	5.34	8.54	38.43	1.72	34.21	3465.57	782.86	2005.86	42.40	0.49	157.22	BDL
	0.23	0.00	12.17	2.49	1.52	17.92	1.06	15.22	1864.84	130.38	550.19	11.29	0.19	29.29	0.00
052606-9-950C	1.90	0.49	64.44	5.94	9.96	46.28	0.53	40.08	3893.21	829.74	1950.23	42.39	0.38	149.68	0.44
	0.19	0.05	15.29	1.69	3.08	15.67	0.18	12.59	1639.18	241.54	200.49	17.05	0.13	26.40	0.00
032206-7-950C	2.40	BDL	59.57	4.53	10.22	55.46	0.90	9.16	6642.56	765.90	2798.68	35.77	0.41	296.87	BDL
	0.25	0.00	8.15	0.83	6.86	10.99	0.37	4.09	1127.67	145.35	623.22	5.04	0.13	47.69	0.00
032206-5-950C	1.74	0.40	62.54	4.65	9.43	50.74	0.53	38.00	3473.76	763.42	1784.78	28.99	0.39	131.16	BDL
	0.28	0.00	10.58	0.65	1.67	24.12	0.25	7.05	2549.76	122.41	406.52	8.53	0.13	33.86	0.00
052606-5-950C-MI1.txt	0.00	BDL	BDL	BDL	BDL	BDL	BDL	BDL	1364.85	497961.56	20.56	BDL	162.44	BDL	BDL
052606-5-950C	0.00	BDL	BDL	BDL	BDL	467.56	BDL	0.85	9983.49	5.69	1.16	3.93	BDL	BDL	BDL
	0.00	0.00	0.00	0.00	0.00	36.90	0.00	0.90	3329.41	1.91	0.46	1.69	0.00	0.00	0.00
052606-10-950C	0.00	BDL	BDL	BDL	2.84	BDL	BDL	0.32	1485.75	511470.34	25.88	BDL	164.23	BDL	BDL
	0.00	0.00	0.00	0.00	0.00	0.00	0.00	0.04	1088.13	17600.88	4.34	0.00	12.47	0.00	0.00
052606-10-950C-MI6.txt	2.14	-	34.02	-	-	54.50	-	5.46	4431.53	1713.26	4976.69	119.46	BDL	328.52	BDL

Table 4A. Average composition of mineral hosts based on LA-ICP-MS (Continued).

Sample:	Te (125)	Ba (138)	La (139)	Ce (140)	Nd (143)	Sm (147)	Eu (153)	Yb (172)	Hf (178)	W (182)	Au (197)	Hg (202)	Pb (208)
010906-1-1kc	3.29	13.33	17.67	65.64	63.74	15.88	3.33	3.08	4.41	0.39	0.33	BDL	0.74
	0.00	25.58	4.71	17.17	15.83	3.75	0.45	1.04	1.24	0.39	0.48	0.00	0.47
050506-26-1kC	BDL	1.44	18.08	66.63	57.93	13.70	2.52	2.87	3.07	0.30	0.26	0.22	0.60
	0.00	1.28	9.29	35.51	27.47	6.29	0.72	1.50	1.64	0.00	0.00	0.14	0.24
050506-28-1kC	BDL	0.17	BDL	0.31	BDL	0.15	BDL	0.10	BDL	0.07	BDL	0.31	0.81
	0.00	0.00	0.00	0.20	0.00	0.11	0.00	0.07	0.00	0.00	0.00	0.12	1.13
052406-6-1kC	BDL	9284.51	3.40	1.62	0.09	0.10	2.35	BDL	0.12	0.14	0.02	0.21	34.37
	0.00	4594.55	0.78	0.33	0.00	0.00	0.81	0.00	0.05	0.00	0.00	0.14	2.48
011906-4-1kC	BDL	4.87	27.77	103.05	99.66	25.14	2.84	7.07	3.19	0.15	BDL	0.58	1.85
	0.00	6.41	3.86	11.45	12.00	5.53	0.50	1.43	1.12	0.00	0.00	0.00	1.71
042806-9-1kC	BDL	34.68	3716.12	8260.29	4028.61	584.69	76.80	54.77	BDL	0.75	BDL	1.48	9.52
	0.00	7.96	780.50	1692.61	762.92	115.76	15.54	12.15	0.00	0.45	0.00	1.37	3.43
042806-9-1kC	BDL	0.12	0.16	39.55	4.53	6.05	1.40	191.78	9459.02	BDL	10.81	BDL	0.37
	0.00	0.04	0.00	17.95	2.92	3.27	0.54	154.24	258.20	0.00	0.65	0.00	0.04
042606-10-950C	BDL	0.62	24.03	100.33	103.89	29.37	1.88	13.44	2.07	0.24	BDL	BDL	1.22
	0.00	0.78	4.31	14.15	14.63	4.66	0.58	3.43	0.65	0.17	0.00	0.00	0.65
042606-14-950C	4.89	0.12	0.89	24.35	3.02	4.36	0.98	192.92	9032.29	0.12	9.52	0.29	1.48
	0.00	0.04	0.64	9.08	1.78	2.13	0.61	61.05	791.27	0.00	1.04	0.08	4.39
042606-14-950C-MI8.txt	BDL	2.80	305.15	515.85	142.95	18.73	5.74	1.77	BDL	5.86	BDL	BDL	2.03
052606-13-950C	0.25	40.05	3869.82	11190.99	6166.66	1119.14	100.35	285.42	118.08	12.72	1.01	0.09	3.81
	0.00	4.41	1000.51	1101.23	1809.81	470.24	65.68	93.45	86.51	8.71	0.61	0.02	1.06
052606-14-950C	BDL	39.82	3774.41	11380.02	6299.91	1158.99	152.05	294.74	49.21	1.46	0.44	0.23	2.89
	0.00	6.52	390.96	2015.80	2268.05	546.77	49.34	91.74	6.57	0.35	0.10	0.24	1.63
052606-11-unheated	BDL	40.90	4138.85	11656.18	6144.80	1114.05	139.96	286.30	53.75	1.61	0.43	0.11	2.93
	0.00	6.31	665.77	1803.44	2600.49	699.77	68.73	95.47	9.30	0.67	0.14	0.00	1.62
052606-9-950C	BDL	46.51	4299.14	13378.69	7655.72	1448.31	184.02	335.45	58.88	2.02	0.43	0.14	3.36
	0.00	6.07	378.71	1856.53	2489.55	698.50	67.17	95.39	14.24	1.48	0.10	0.11	2.14
032206-7-950C	BDL	42.57	3605.78	12282.74	7549.03	1597.57	118.19	537.68	62.01	1.74	0.73	BDL	3.49
	0.00	3.09	321.10	890.01	1531.63	491.14	45.01	45.67	15.83	0.44	0.23	0.00	1.50
032206-5-950C	BDL	45.93	4913.69	12610.41	6743.19	1167.58	160.70	287.43	54.41	1.43	0.39	0.17	2.49
	0.00	8.47	1062.97	2527.52	3118.11	809.45	75.91	162.89	7.65	0.61	0.17	0.11	0.45
052606-5-950C-MI1.txt	BDL	BDL	BDL	43.95	4.75	9.44	2.34	368.47	8691.66	BDL	8.37	BDL	0.31
052606-5-950C	BDL	1456.60	264383.54	383742.00	80237.01	7258.80	39.39	207.75	0.36	6.25	BDL	BDL	86.77
	0.00	31.69	19549.16	5668.21	5953.84	1329.27	10.42	75.21	0.10	2.57	0.00	0.00	13.39
052606-10-950C	BDL	0.25	0.84	74.13	5.79	8.29	1.97	480.31	10382.23	0.17	10.00	BDL	1.12
	0.00	0.17	0.00	67.98	4.93	9.01	1.84	275.36	1447.15	0.00	1.45	0.00	0.35
052606-10-950C-MI6.txt	BDL	45.69	4225.29	12559.73	7463.44	1380.44	89.65	380.14	224.84	7.41	1.66	BDL	5.03

Table 4A. Average composition of mineral hosts based on LA-ICP-MS (Continued).

Sample:	Bi (209)	Th (232)	U (238)
010906-1-1kc	0.03	0.38	0.08
	0.02	0.34	0.06
050506-26-1kC	0.05	0.30	0.06
	0.01	0.17	0.03
050506-28-1kC	0.01	BDL	0.03
	0.00	0.00	0.02
052406-6-1kC	0.01	BDL	0.04
	0.00	0.00	0.03
011906-4-1kC	BDL	0.27	0.10
	0.00	0.14	0.12
042806-9-1kC	0.21	87.85	11.99
	0.11	26.35	3.56
042806-9-1kC	BDL	168.25	118.47
	0.00	54.62	68.09
042606-10-950C	0.16	0.39	0.17
	0.10	0.40	0.13
042606-14-950C	BDL	90.02	64.94
	0.00	48.13	67.79
042606-14-950C-MI8.txt	2.22	1.46	1.83
052606-13-950C	1.32	589.74	204.86
	0.80	243.64	151.39
052606-14-950C	0.14	420.42	27.72
	0.05	58.68	3.50
052606-11-unheated	0.17	457.06	29.69
	0.11	74.36	11.01
052606-9-950C	0.16	503.42	36.18
	0.07	58.02	6.33
032206-7-950C	0.23	332.06	24.06
	0.08	74.39	4.51
032206-5-950C	0.19	411.62	25.93
	0.17	168.72	20.74
052606-5-950C-MI1.txt	BDL	129.37	50.64
052606-5-950C	0.39	84786.36	488.14
	0.12	16398.90	137.62
052606-10-950C	BDL	673.47	270.88
	0.00	486.42	181.32
052606-10-950C-MI6.txt	0.99	1141.55	131.23

Table 4B. Electron microprobe analysis of apatites in wt %.

Sample	Unit	Average	SiO2	FeO	K2O	Na2O	Al2O3	MnO	Cr2O3	MgO	TiO2
010906-1-2-Apat_Inc	Trachyandesite Post-ore	n=5	0.455	0.429	0.019	0.145	0.017	0.085	0.004	0.464	0.013
		Stdev	0.247	0.089	0.005	0.013	0.035	0.018	0.003	0.077	0.019
050506-26-10-Apat_Inc	Trachyandesite Post-ore	n=1	0.434	0.575	0.002	0.068	0.020	0.059	0.020	0.296	0.075
052406-6-Apat_inc4	Pre-ore Trachydacite	n=6	0.586	0.192	0.048	0.203	0.017	0.187	0.001	0.058	0.010
		Stdev	0.228	0.087	0.045	0.084	0.020	0.046	0.002	0.024	0.019
042806-9-002-6-Apatite_Host	Dated trachydacite porphyry	n=32	0.315	0.064	0.004	0.167	0.005	0.056	0.005	0.064	0.004
		Stdev	0.107	0.037	0.007	0.050	0.007	0.036	0.011	0.023	0.008
042606-10	**Dated pluton roof**	n=3	0.664	0.194	0.009	0.200	0.010	0.118	0.000	0.077	0.000
		Stdev	0.066	0.010	0.007	0.015	0.011	0.017	0.000	0.004	0.000
042606-10_Inc	**Dated pluton roof**	n=7	0.574	0.409	0.007	0.363	0.002	0.089	0.000	0.094	0.024
		Stdev	0.057	0.060	0.014	0.111	0.003	0.030	0.000	0.023	0.039
042606-10-001-Apat1	**Dated pluton roof**	n=29	0.416	0.138	0.005	0.318	0.005	0.055	0.000	0.098	0.010
		Stdev	0.137	0.049	0.008	0.083	0.007	0.041	0.001	0.024	0.016
042606-14	Reddish pluton roof	n=34	0.388	0.061	0.008	0.344	0.077	0.120	0.000	0.043	0.008
		Stdev	0.105	0.030	0.013	0.064	0.389	0.046	0.001	0.027	0.017
052606-13insphene17	Upper Qz monzonite near granite	n=2	0.450	0.095	0.007	0.258	0.004	0.107	0.000	0.022	0.000
		Stdev	0.033	0.057	0.009	0.057	0.001	0.050	0.000	0.004	0.000
052606-9-Apat_included	Coarse grained middle granite	n=1	0.361	0.048	0.000	0.204	0.000	0.110	0.000	0.019	0.164
032306-3a-Apat_Inc	Lower quartz monzonite	n=12	0.394	0.473	0.022	0.176	0.026	0.093	0.005	0.260	0.032
		Stdev	0.146	0.191	0.032	0.032	0.054	0.036	0.009	0.101	0.032
032306-5-Apat1	Folliated mafic lower Qz monzonite	n=33	0.472	0.015	0.005	0.139	0.008	0.051	0.001	0.009	0.012
		Stdev	0.163	0.019	0.008	0.070	0.009	0.040	0.004	0.009	0.020
052606-10-Apat1	Late quartzite	n=11	0.312	0.051	0.005	0.192	0.008	0.267	0.006	0.010	0.015
		Stdev	0.134	0.034	0.008	0.134	0.009	0.149	0.008	0.014	0.020

Table 4B. Electron microprobe analysis of apatites (Continuation).

Sample	CaO	V2O3	P2O5	Cl	F	SO3	Total
010906-1-2-Apat_Inc	55.483	0.012	43.986	0.203	3.819	0.279	103.758
	0.947	0.021	0.585	0.097	0.118	0.029	1.117
050506-26-10-Apat_Inc	53.252	0.000	44.723	0.214	3.731	0.292	102.142
052406-6-Apat_inc4	52.754	0.000	42.991	0.447	3.316	0.408	99.720
	0.891	0.000	1.577	0.047	0.170	0.186	2.166
042806-9-002-6-Apatite_Host	55.139	0.010	43.181	0.312	3.720	0.185	101.595
	0.841	0.018	0.858	0.243	0.202	0.091	1.144
042606-10	51.677	0.001	42.167	1.232	3.786	0.119	98.382
	0.324	0.002	1.150	0.010	0.118	0.061	1.001
042606-10_Inc	51.873	0.001	43.037	0.922	3.691	0.367	99.689
	0.717	0.002	0.427	0.160	0.179	0.144	0.880
042606-10-001-Apat1	54.297	0.002	42.689	0.937	3.916	0.419	101.444
	0.526	0.011	1.013	0.402	0.149	0.188	0.919
042606-14	51.896	0.005	43.119	0.206	3.297	0.429	98.566
	0.504	0.011	0.738	0.065	0.115	0.133	0.810
052606-13insphene17	54.204	0.000	43.271	1.104	4.341	0.387	102.170
	0.723	0.000	0.115	0.139	0.069	0.150	0.897
052606-9-Apat_included	51.827	0.000	43.056	0.012	3.846	0.437	98.462
032306-3a-Apat_Inc	52.266	0.026	43.354	0.382	3.841	0.526	100.172
	0.634	0.028	0.828	0.137	0.129	0.089	1.067
032306-5-Apat1	53.235	0.020	43.244	0.282	3.612	0.305	99.824
	0.495	0.026	0.878	0.085	0.135	0.140	1.053
052606-10-Apat1	52.891	0.010	43.745	0.011	3.579	0.285	99.879
	0.845	0.019	0.998	0.011	0.095	0.271	1.086

Table 5A. Average composition of melt inclusions in wt % based on electron microprobe analysis.

Sample	Average	Comment	SiO2	Al2O3	MgO	FeO	TiO2	MnO	CaO	Na2O	K2O	P2O5	SO3	F	Cl	Cr2O3	V2O3	Water	Total
010906-1-1000C	n=27	Trachyandesite post-mineral	66.7	18.4	0.47	0.99	0.76	0.03	1.72	4.62	5.99	0.57	0.038	0.034	0.048	0.010	0.018	0.0	100.4
	Stdev		1.4	0.9	0.31	0.30	0.20	0.03	0.55	0.93	0.77	0.25	0.021	0.018	0.019	0.014	0.023		1.3
050506-26-1000C	n=22	Trachyandesite post-mineral	68.3	17.5	0.46	1.56	0.79	0.04	1.68	4.03	5.64	0.39	0.063	0.022	0.076	0.019	0.012	0.0	100.6
	Stdev		2.7	1.3	0.32	0.60	0.14	0.03	0.52	0.47	1.09	0.26	0.033	0.017	0.018	0.032	0.021		1.0
011906-4-1000C	n=18	Black trachydacite big hill South of Quartette Pre-ore	74.0	14.3	0.34	1.38	0.42	0.02	1.07	3.49	6.06	0.15	0.037	0.013	0.089	0.007	0.016	0.0	101.4
	Stdev		1.5	0.4	0.35	0.67	0.08	0.03	0.84	0.45	0.77	0.38	0.029	0.023	0.032	0.010	0.021		1.3
042806-9-1000C	n=20	Dated trachydacite porphyry	70.4	12.3	0.55	1.36	0.13	0.03	0.82	2.77	5.41	0.10	0.019	0.009	0.111	0.000	0.005	6.0	100.0
	Stdev		1.6	0.4	0.60	0.64	0.01	0.00	0.22	0.45	0.39	0.15	0.006	0.013	0.064	0.000	0.007		1.3
042606-10-950C	n=11	Dated pluton roof	75.8	12.5	0.38	0.66	0.06	0.04	0.86	3.08	5.46	0.03	0.009	0.002	0.215	0.012	0.019	0.9	100.0
	Stdev		2.9	1.8	0.34	0.40	0.11	0.03	0.41	0.96	1.11	0.03	0.009	0.004	0.189	0.015	0.020		3.0
042606-10-950C	n=2	Dated pluton roof	84.0	7.7	0.93	1.07	0.04	0.02	1.71	1.04	3.41	0.00	0.035	0.000	0.217	0.012	0.013	0.0	100.1
	Stdev		5.1	1.2	0.28	0.54	0.06	0.01	0.07	0.94	0.75	0.00	0.043	0.000	0.141	0.008	0.018		3.0
042606-14-950C	n=7	Reddish pluton roof	70.8	14.7	0.11	0.84	0.21	0.02	0.54	3.75	6.46	0.01	0.026	0.002	0.122	0.005	0.012	2.4	100.0
	Stdev		2.0	1.7	0.06	0.60	0.27	0.03	0.21	0.64	0.72	0.03	0.020	0.004	0.015	0.011	0.020		1.4
052606-13-950C	n=2	Upper monzonite, lower sector near granite	74.7	13.0	0.05	0.49	0.57	0.04	0.94	2.51	5.52	0.00	0.028	0.000	0.129	0.006	0.060	1.9	100.0
	Stdev		3.1	1.2	0.01	0.30	0.81	0.04	0.80	0.14	0.64	0.00	0.015	0.000	0.084	0.008	0.023		0.7
052606-14-950C	n=15	Limit middle granite/upper unit	73.6	12.1	0.06	0.51	1.16	0.03	1.26	2.31	4.89	0.03	0.012	0.005	0.074	0.004	0.027	3.9	100.0
	Stdev		3.0	2.6	0.03	0.22	0.49	0.03	0.34	1.36	1.05	0.03	0.015	0.008	0.048	0.007	0.029		3.4
052606-14-950C	n=2	Limit middle granite/upper unit, other population	83.4	11.2	0.01	0.09	0.31	0.01	0.47	3.73	4.06	0.00	0.006	0.007	0.008	0.016	0.014	0.0	103.3
	Stdev		4.6	2.2	0.00	0.11	0.05	0.02	0.02	1.42	1.16	0.00	0.008	0.001	0.001	0.022	0.020		0.2
052606-9-950C	n=7	Coarse grained granite, middle unit	73.4	11.9	0.04	0.41	1.17	0.06	1.24	2.17	4.27	0.05	0.014	0.006	0.094	0.008	0.052	5.1	100.0
	Stdev		1.3	1.2	0.03	0.13	0.78	0.03	0.62	0.91	0.37	0.11	0.017	0.008	0.025	0.008	0.034		2.7
032206-7-950C	n=14	Middle granite unit, deep area	74.2	12.4	0.06	0.44	0.95	0.04	1.04	2.59	5.16	0.01	0.016	0.007	0.053	0.012	0.033	2.9	100.0
	Stdev		2.9	2.0	0.05	0.26	0.47	0.03	0.41	0.66	1.15	0.03	0.013	0.008	0.034	0.014	0.031		2.2
032206-5-950C	n=6	K-feldspar phyric lower quartz monzonite	74.7	13.2	0.04	0.28	0.37	0.01	0.82	3.67	3.65	0.03	0.045	0.008	0.048	0.006	0.009	3.1	100.0
	Stdev		2.3	2.2	0.03	0.25	0.36	0.01	0.35	1.93	1.66	0.04	0.073	0.009	0.034	0.010	0.011		5.3
052606-5-950C	n=2	Recrystallized middle unit, very small	83.9	8.0	0.02	0.05	0.02	0.10	0.11	1.15	3.54	0.09	0.018	0.016	0.016	0.022	0.000	3.0	100.0
	Stdev		5.1	2.9	0.02	0.00	0.03	0.14	0.12	1.40	0.43	0.11	0.025	0.014	0.006	0.001	0.000		0.7

Table 5B. Average composition of melt inclusions based on LA-ICP-MS. Oxides in wt %, isotopes in parenthesis in ppm.

Sample:	Comments	No.	Na2O	MgO	Al2O3	SiO2	K2O	CaO	TiO2	V (51)	Cr (52)	MnO	FeO	Co (59)	Ni (62)	Cu (63)	Zn (66)	As (75)
010906-1-1kc	Trachyandesite post-mineral	n=21	5.2	0.58	21.3	62.4	6.4	1.61	0.91	85.8	13.0	0.04	1.39	7.3	50.9	73.4	48.8	8.4
		Stdev	0.6	0.48	1.3	1.8	1.0	0.78	0.22	37.7	6.2	0.03	0.93	3.9	39.2	42.9	36.5	2.0
050506-26-1kC	Trachyandesite post-mineral	n=17	5.3	0.38	19.6	65.8	5.2	1.35	0.77	70.0	374.2	0.03	1.14	11.5	24.1	111.1	59.7	13.7
		Stdev	0.6	0.24	1.7	2.8	1.1	0.73	0.16	34.2	275.6	0.01	0.43	12.0	0.0	87.0	39.5	15.6
050506-28-1kC	Obsidian, syn-ore.	n=13	3.2	0.04	13.0	78.2	4.4	0.42	0.10	1.5	2.5	0.04	0.58	19.0	29.5	11.4	28.7	12.1
		Stdev	0.2	0.01	0.0	0.5	0.3	0.02	0.02	0.7	2.0	0.00	0.18	3.1	17.5	14.0	8.5	17.5
050506-28-1kC-MI7	Obsidian, syn-ore.		3.4	0.02	13.0	77.7	4.6	0.40	0.13	16.3	21.7	0.06	0.51	186.7	BDL	BDL	BDL	285.2
052406-6-1kC	Fresh Trachydacite, premineral (near flow banded)	n=13	2.5	0.04	14.8	73.4	8.1	0.26	0.09	2.5	1.6	0.02	0.45	BDL	31.6	3.7	12.4	4.0
		stdev	0.3	0.01	0.9	1.5	0.7	0.08	0.02	1.6	0.0	0.00	0.08	0.0	37.3	2.5	4.2	2.7
052406-6-1kC-MI19, altered	Fresh Trachydacite, premineral (near flow banded)	n=1	3.9	11.89	15.0	71.1	BDL	1.15	0.54	1624.6	BDL	0.07	9.47	8.2	BDL	86.0	156.2	9.9
011906-4-1kC	Black trachydacite big hill South of Quartette Pre-ore	n=6	3.1	0.11	14.9	75.0	6.5	0.77	0.49	76.4	BDL	0.02	1.30	11.5	78.2	12.7	196.5	34.2
		Stdev	0.5	0.08	0.4	2.2	0.4	0.70	0.09	31.4	0.0	0.01	0.83	0.0	0.0	0.0	100.0	0.0
042806-9-1kC	Dated trachydacite porphyry	n=2	3.8	1.88	14.6	69.9	4.3	0.52	0.10	38.0	0.9	0.16	4.40	14.9	136.2	59.4	49.8	38.1
		stdev	1.3	1.73	1.0	0.2	0.7	0.69	0.06	0.0	0.0	0.00	0.33	0.0	135.6	19.2	0.0	39.5
042806-9-1kC, altered	Dated trachydacite porphyry	n=8	2.9	9.76	12.5	62.7	3.6	1.00	0.09	17.1	2.0	0.27	5.88	25.5	51.0	80.2	98.7	55.2
		stdev	0.5	2.00	1.4	2.8	1.7	0.00	0.04	25.7	1.4	0.14	2.31	19.9	19.1	115.8	34.1	58.9
042606-10-950C	Dated pluton roof	n=4	2.9	0.71	13.3	76.1	5.0	2.59	0.12	69.2	22.1	0.12	1.31	44.5	221.7	5.4	66.0	274.8
		Stdev	0.1	0.24	0.6	3.7	0.5	1.46	0.10	71.3	30.6	0.14	0.62	0.0	0.0	1.5	0.0	182.3
042606-14-950C	Reddish pluton roof	n=14	3.3	0.13	16.4	72.1	5.8	0.91	0.25	14.5	1.8	0.02	0.68	16.6	12.0	76.7	37.3	13.9
		Stdev	0.7	0.07	2.5	3.8	1.0	0.62	0.13	5.1	1.0	0.01	0.33	14.1	9.9	43.6	33.2	13.2
042606-14-950C	Reddish pluton roof	n=5	1.5	0.07	8.1	86.1	2.8	0.35	0.19	9.7	4.7	0.01	0.44	BDL	79.9	28.2	16.0	23.9
		Stdev	0.4	0.02	1.9	3.1	0.6	0.08	0.04	7.1	2.5	0.01	0.10	0.0	0.0	7.2	0.0	10.6
052606-14-950C	Limit middle granite/upper unit	n=7	3.2	0.07	13.3	78.6	4.8	1.41	1.00	74.9	66.6	0.06	0.71	2.4	53.9	18.4	11.5	36.1
		Stdev	0.7	0.02	2.0	3.8	0.6	0.47	0.00	55.5	108.0	0.03	0.40	0.5	5.4	24.3	3.1	54.4
052606-11-unheated	Middle granite unit, upper part	n=4	3.3	0.07	15.0	74.7	5.2	1.36	0.40	72.7	BDL	0.03	0.75	BDL	75.5	7.7	20.2	63.9
		stdev	0.8	0.02	2.3	1.6	0.7	0.62	0.00	35.3	0.0	0.03	0.89	0.0	0.0	2.5	9.8	60.3
052606-11-unheated	Middle granite unit, upper part	n=3	2.0	0.03	9.1	86.5	3.3	2.50	0.40	165.1	12.0	0.12	1.05	BDL	11.1	BDL	14.4	24.7
		stdev	0.3	0.04	2.6	4.8	1.2	0.00	0.00	83.8	0.8	0.05	0.67	0.0	0.0	0.0	0.0	0.0
052606-9-950C	Coarse grained granite, middle unit	n=6	3.4	0.18	14.5	77.2	5.4	BDL	0.30	67.2	3.7	0.04	0.77	1.9	23.1	40.0	20.8	35.1
		stdev	0.6	0.16	1.6	2.6	0.8	0.00	0.00	77.9	0.5	0.03	0.18	0.2	18.5	24.4	2.6	17.8
032206-7-950C	Middle granite unit, deep area	n=9	4.3	0.10	18.0	69.2	5.9	0.91	1.00	536.7	71.3	0.10	0.40	9.6	82.4	18.2	35.4	74.5
		stdev	0.8	0.07	3.1	6.1	0.9	0.47	0.00	472.8	0.0	0.00	0.00	11.8	108.8	22.8	35.0	51.1
032206-5-950C	K-feldspar phyric lower quartz monzonite	n=9	3.1	0.10	15.1	72.3	5.3	2.52	1.00	77.7	32.9	0.05	0.99	1.8	63.2	10.9	16.1	109.6
		Stdev	0.8	0.04	1.9	3.8	0.9	0.51	0.00	77.0	0.0	0.03	0.91	0.0	61.1	11.0	11.5	59.8
032206-5-950C	K-feldspar phyric lower quartz monzonite	n=4	2.6	0.03	12.0	83.8	3.9	0.40	0.78	83.2	BDL	0.08	0.85	BDL	13.4	7.9	16.0	36.9
		Stdev	0.5	0.03	1.3	3.6	0.7	0.00	0.44	109.2	0.0	0.05	0.67	0.0	0.0	3.6	10.0	0.0
052606-5-950C	Recrystallized middle unit	n=3	3.3	0.02	15.1	75.0	4.2	BDL	0.02	BDL	4.3	0.16	0.05	42.9	416.0	26.6	93.0	4920.9
		Stdev	0.9	0.00	2.8	0.0	0.5	0.00	0.01	0.0	0.0	0.15	0.04	0.0	0.0	16.3	68.5	6453.0
052606-5-950C	Recrystallized middle unit	n=1	3.9	0.01	17.1	71.4	5.8	1.24	0.21	8.1	BDL	0.04	0.18	BDL	BDL	21.8	15.1	BDL

Table 5B *(continued)*. Average composition of melt inclusions based on LA-ICP-MS.

Sample:	Rb (85)	Sr (88)	Y (89)	Zr (90)	Nb (93)	Mo (98)	Ag (107)	Sn (120)	Sb (121)	Te (125)	Ba (138)	La (139)	Ce (140)	Nd (143)	Sm (147)	Eu (153)	Yb (172)	Hf (178)
010906-1-1kc	166.1	1025.7	23.0	575.5	33.2	3.1	0.74	2.5	0.6	1.5	0.3	114.5	228.6	83.0	13.2	3.2	2.4	16.1
	34.6	333.4	17.6	113.7	5.3	1.4	0.73	0.7	0.0	1.2	0.1	28.0	71.7	46.0	9.0	1.5	1.6	5.3
050506-26-1kC	175.1	583.5	17.6	488.5	35.2	3.4	0.24	1.9	2.2	9.2	1482.4	108.0	214.4	70.9	8.5	1.5	2.1	10.8
	49.6	318.1	9.4	181.0	10.7	1.5	0.05	0.7	1.2	2.2	919.0	44.3	102.5	34.8	4.6	0.6	1.0	4.7
050506-28-1kC	164.5	9.7	12.5	85.4	23.6	4.9	1.55	2.2	2.5	55.6	12.4	31.4	51.1	9.9	3.3	0.2	1.6	3.6
	12.2	2.4	2.4	16.4	4.9	3.2	1.34	1.8	3.4	0.0	3.4	3.0	4.0	3.4	4.8	0.1	0.7	0.7
050506-28-1kC-MI7	373.3	16.5	21.2	97.3	22.7	BDL	24.03	BDL	BDL	120.8	14.3	24.1	34.0	BDL	39.4	6.9	8.7	22.0
052406-6-1kC	128.6	258.3	8.6	67.8	13.0	2.4	1.22	1.2	0.9	12.2	3360.4	32.3	51.9	13.3	2.1	1.2	1.1	2.4
	8.4	85.3	4.5	20.2	3.9	1.5	0.86	0.8	0.6	15.3	2054.4	8.4	15.9	6.6	1.2	0.8	0.5	0.9
052406-6-1kC-MI19, altered	475.8	BDL	3.0	162.1	25.4	0.1	BDL	22.5	2.2	BDL	BDL	54.7	107.3	20.2	2.0	BDL	0.4	12.1
011906-4-1kC	194.5	122.3	15.4	366.0	24.1	6.4	BDL	3.0	BDL	115.3	780.1	57.3	104.5	23.9	1.0	1.6	4.9	12.0
	8.7	49.3	3.8	33.1	3.3	6.0	0.00	0.0	0.0	0.0	398.6	13.4	6.6	11.3	0.0	1.3	3.5	1.6
042806-9-1kC	570.1	BDL	BDL	96.1	7.0	11.1	BDL	9.0	BDL	5.2	2998.2	387.7	BDL	2163.9	640.5	19.3	8.2	2.9
	604.3	0.0	0.0	0.0	7.1	11.4	0.00	11.5	0.0	0.0	576.3	0.0	0.0	0.0	0.0	0.0	0.0	0.0
042806-9-1kC, altered	216.0	768.6	505.2	79.9	7.9	7.3	5.69	2.2	1.9	25.8	2335.1	3175.3	6485.8	1695.9	332.7	30.1	17.6	3.2
	217.0	504.7	0.0	18.3	3.1	9.7	0.00	1.9	0.0	16.1	1521.6	1914.3	2765.8	1649.6	271.9	26.7	22.3	1.1
042606-10-950C	453.7	60.2	18.0	83.0	18.9	20.9	BDL	1.1	30.9	BDL	27.7	27.4	54.8	34.5	BDL	3.7	1.1	3.8
	131.4	31.6	5.4	60.1	7.9	1.2	0.00	0.0	17.7	0.0	5.9	15.4	33.3	13.7	0.0	0.0	0.0	1.8
042606-14-950C	168.9	203.3	1540.4	237.7	19.7	5.0	51.94	1.7	10.6	53.9	909.9	88.8	143.8	67.2	16.5	2.5	413.7	3851.3
	61.1	312.6	2320.4	70.4	7.4	2.2	21.00	0.9	8.5	43.3	1419.3	55.1	98.0	46.0	12.4	3.6	540.1	4994.4
042606-14-950C	85.6	64.3	12.5	257.3	7.5	BDL	BDL	2.2	9.3	80.9	351.6	42.3	38.5	21.4	5.6	2.7	BDL	4987.2
	32.8	21.5	0.0	3.3	3.3	0.0	0.00	0.0	0.0	0.0	159.2	9.0	21.3	12.4	0.0	0.0	0.0	2065.1
052606-14-950C	166.6	50.3	3714.3	244.2	1473.8	29.8	0.47	206.8	0.2	11.4	228.9	231.8	7749.0	14253.4	2000.6	301.4	177.7	31.4
	21.6	12.9	4522.4	247.7	849.0	21.9	0.29	136.2	0.0	0.0	96.7	27.3	BDL	0.0	2666.3	0.0	210.9	14.8
052606-11-unheated	803.9	82.8	2489.9	257.2	1456.4	24.3	2.28	95.4	9.8	10.2	258.3	2880.5	5280.8	7322.2	1295.5	178.8	173.6	14.1
	881.2	24.3	2974.2	96.0	1914.0	18.9	0.70	107.4	0.0	0.0	149.0	0.0	3545.0	7391.1	1574.6	160.7	118.3	18.2
052606-11-unheated	111.0	35.2	1590.7	503.6	1114.4	46.8	1.57	371.3	BDL	20.6	217.6	BDL	1911.4	1953.8	1603.5	136.8	135.0	33.6
	35.8	19.2	1887.3	0.0	781.2	5.6	0.10	84.0	0.0	6.2	51.6	0.0	192.6	2605.0	0.0	0.0	0.0	0.0
052606-9-950C	190.4	83.9	2588.9	410.7	994.2	89.4	2.12	131.3	0.8	1.7	380.8	923.4	2729.7	4758.3	1166.4	143.0	107.5	24.9
	33.2	23.9	1165.3	166.9	521.0	138.1	0.00	52.0	0.1	0.0	268.4	787.7	2576.1	3044.3	636.4	67.6	85.1	16.1
032206-7-950C	245.5	44.8	5031.4	671.0	4357.2	30.6	1.12	391.7	4.7	BDL	153.6	3441.7	8587.5	9485.8	3482.1	190.1	364.9	104.7
	91.1	59.3	9617.9	834.0	4733.0	29.7	0.67	161.8	5.9	0.0	219.5	2868.5	6853.5	8039.9	3123.3	177.4	609.2	113.7
032206-5-950C	142.6	106.0	6684.8	677.2	3099.5	25.6	1.79	115.0	6.8	18.7	317.0	1669.8	10398.3	14290.2	3481.3	372.9	499.4	40.6
	25.9	28.3	4749.6	542.2	1749.0	36.9	1.02	93.4	8.8	0.0	97.5	708.5	10370.7	9747.7	2557.4	249.2	274.9	23.0
032206-5-950C	106.8	48.1	3251.1	502.8	515.1	36.1	1.02	103.8	1.8	19.6	184.7	761.3	664.4	1909.2	493.8	46.1	378.1	59.0
	25.1	14.0	2665.8	501.8	683.8	27.8	0.00	170.0	0.0	10.7	98.1	746.9	597.4	2677.3	693.4	62.9	90.5	0.0
052606-5-950C	961.1	8.7	BDL	108.7	24.7	BDL	6.61	24.4	85.3	141.8	1068.9	BDL	230189.2	381247.2	51934.0	167.6	BDL	25.3
	149.5	7.6	0.0	0.0	28.8	0.0	0.00	0.0	36.4	0.0	0.0	0.0	265227.5	493713.1	68041.2	201.8	0.0	18.7
052606-5-950C	134.1	123.3	685.7	61.8	25.7	2.4	29.80	2.1	BDL	6.3	1028.1	126.6	255.6	98.1	13.8	2.2	196.9	BDL

Table 5B *(Continued)*. Average composition of melt inclusions based on LA-ICP-MS.

Sample:	W (182)	Au (197)	Hg (202)	Pb (208)	Bi (209)	Th (232)	U (238)
010906-1-1kc	2.6	0.15	0.18	36.2	0.20	28.9	6.7
	1.2	0.14	0.00	8.2	0.09	6.9	1.7
050506-26-1kC	2.3	0.17	0.49	36.4	0.31	35.1	7.0
	1.4	0.12	0.05	7.2	0.14	13.4	2.8
050506-28-1kC	2.5	1.77	2.03	31.6	0.16	29.6	5.2
	0.7	3.61	4.27	3.3	0.07	3.3	0.6
050506-28-1kC-MI7	34.3	19.90	66.15	210.3	BDL	42.1	1.9
052406-6-1kC	1.0	0.84	1.81	34.9	0.12	15.8	2.5
	0.3	0.00	2.14	10.9	0.07	2.9	0.5
052406-6-1kC-MI19, altered	0.8	BDL	108.96	BDL	BDL	86.7	14.2
011906-4-1kC	1.6	BDL	13.37	31.4	1.23	29.5	7.5
	0.0	0.00	0.00	8.9	1.40	3.8	3.0
042806-9-1kC	2.6	0.13	BDL	14.6	BDL	9.6	10.9
	0.0	0.00	0.00	14.9	0.00	8.3	7.8
042806-9-1kC, altered	2.3	0.18	1.50	17.7	0.46	63.5	7.5
	1.4	0.00	0.84	9.2	0.20	79.2	6.0
042606-10-950C	19.6	BDL	BDL	45.3	3.81	30.9	57.7
	4.7	0.00	0.00	7.3	2.88	34.7	24.0
042606-14-950C	4.1	5.27	1.52	31.3	0.47	208.1	91.7
	5.5	6.16	1.44	8.8	0.59	297.6	104.5
042606-14-950C	1.7	11.58	1.69	13.6	0.62	18.0	5.8
	0.0	13.76	0.47	5.2	0.00	0.0	8.2
052606-14-950C	2.5	0.51	0.51	17.0	0.43	160.5	10.3
	1.0	0.46	0.17	7.4	0.34	91.2	4.7
052606-11-unheated	4.0	0.75	BDL	25.1	1.08	243.5	10.2
	1.6	0.00	0.00	6.2	0.59	301.6	5.8
052606-11-unheated	4.3	0.50	0.70	21.5	0.86	134.3	8.2
	1.8	0.00	0.55	6.7	0.21	19.3	0.1
052606-9-950C	11.4	0.33	0.15	64.1	0.21	188.6	25.9
	13.7	0.22	0.10	67.2	0.08	77.7	22.2
032206-7-950C	4.1	1.40	0.64	49.0	0.37	251.7	9.6
	2.9	1.09	0.82	27.5	0.32	370.8	14.0
032206-5-950C	3.1	1.03	1.49	23.5	0.48	309.4	16.7
	2.5	0.67	0.96	7.7	0.22	50.4	12.2
032206-5-950C	2.0	1.54	BDL	24.1	0.42	184.0	23.3
	1.6	0.00	0.00	3.3	0.37	164.2	20.7
052606-5-950C	12.7	5.83	3.14	1223.0	43.25	1478165.3	13306.6
	1.1	0.00	0.00	1727.9	70.69	2497599.0	15906.6
052606-5-950C	1.1	BDL	0.88	27.2	0.10	289.4	98.6

Table 6. Summary of melt inclusion results based on electron microprobe and LA-ICP-MS.

Sample Code	Rock unit	Macroscopic Description	Location	Age (Ma)	Mineral host of MI	Melt inclusion composition
011906-4	pre-ore volcanic rock	black flow banded trachydacite, consisting of blocks of up to 2m in diameter. It is Plag-Biot-phyric trachydacite with a gray-pink matrix.	3.5 km south of the Quartette mine	16.9 ± 0.5 (1)	clinopyroxene	rhyolite
052406-6	pre-ore volcanic rock	small plug or dome of rhyolite that cut older trachyandesites. Consist of a quartz-biotite phyric rhyolite	Near the Blossom mine	16.9 ± 0.2 (1)	clinopyroxene	rhyolite
042806-9	pre-ore subvolcanic rock	widespread trachydacite porphyry that intrudes older volcanic rocks and hosts most of the mineralization. Consist of a Plag-Hb-phyric trachydacite porphyry, moderately altered to Epdt, clay, chlorite, calcite, and sericite.	Near the Quartette mine	17.1 ± 0.2 (1)	apatite and zircon	high silica trachydacite
050506-28	syn-ore volcanic rock	obsidian from Rhyolite lavas (Thr). Mostly glass with rare quartz, plagioclase and sanidine	Southern part of Highland Range South	16.26 ± 0.15 (2)	quartz and sanidine	rhyolite
042606-10	upper quartz-monzonite (roof)	moderately altered quartz-monzonite, intrudes trachydacite porphyry. Weakly to Mod. Altered to actinolite.	Near the Quartette mine	16.6 ± 0.9 (1)	clinopyroxene	rhyolite
042606-14	upper quartz-monzonite	reddish quartz-monzonite at 550 m from the roof. Weakly to Mod. Altered to actinolite.	North of the town of Searchlight	NA	zircon	low silica rhyolite
052606-13	upper quartz-monzonite	Coarse grained quartz monzonite near the limit with the middle granite	4.8 km northeast of Searchlight	NA	sphene	rhyolite
052606-14	middle granite	Coarse grained plag-K-feldspar-phyric granite with sphene	5 km northeast of Searchlight	NA	sphene	rhyolite
052606-11	middle granite	Coarse grained Plag-Biot-K-feldspar-Phyric granite with sphene. Most K-feldspar and quartz are in the ground mass.	5.1 km northeast of Searchlight	NA	sphene	rhyolite
052606-9	middle granite	Coarse grained K-feldspar-Plag-Phyric granite with abundant sphene.	5.8 km northeast of Searchlight	NA	sphene	rhyolite
052606-5	middle granite	Coarse grained granite granite containing biotite and muscovite and Myarolithic cavities and hematite stains.	6 km northeast of Searchlight	NA	zircon amd xenotime	high silica rhyolite
032206-7	middle granite, deep area	Coarse grained myarolithic granite	7 km northeast of Searchlight	NA	sphene	rhyolite
032206-5	lower cumulate quartz-monzonite	Coarse grained K-feldspar-Phyric quartz-monzonite with K-feldspar of ~2 cm long	8.3 km northeast of Searchlight	NA	sphene	rhyolite
010906-1	post-ore volcanic rock	Vessicular black trachyandesite from basaltic andesite lavas (Thb) deposited on top of tuffs.	Northern part of Highland Range South	15.98 ± 0.05 (2)	clinopyroxene	trachydacite
050506-26	post-ore volcanic rock	Vessicular black trachyandesite from basaltic andesite lavas (Thb) deposited on top of tuffs.	Southern part of Highland Range South	15.66 ± 0.08 (2)	clinopyroxene	trachydacite

(1) (Lledo et al., 2009)
(2) (Faulds et al. 2002b)

Table 6. Summary of melt inclusion results based on electron microprobe and LA-ICP-MS (continued).

Sample Code	water wt %	SO3 wt %	F wt %	Cl wt %	Cu ppm	Zn ppm	As ppm	Mo ppm	Sn ppm	Hg ppm	Ag ppm	Au ppm	Pb ppm
011906-4	BDL	0.037	0.013	0.089	12.7	197.0	34.0	6.4	3.0	13.0	BDL	BDL	31.0
052406-6					3.7	12.0	4.0	2.4	1.2	1.8	1.2	0.8	35.0
042806-9	6	0.019	0.009	0.11	59.0	50.0	38.0	11.0	9.0	BDL	BDL	0.1	14.6
050506-28					11.0	29.0	12.0	4.9	2.2	2.0	1.5	1.8	32.0
042606-10	0.9	0.009	0.0025	0.21	5.4	66.0	274.0	21.0	1.1	BDL	BDL	BDL	45.0
042606-14	2.44	0.026	0.0024	0.12	77.0	37.0	14.0	5.0	1.7	1.5	52.0	5.3	31.0
052606-13	1.92	0.028	BDL	0.13									
052606-14	3.93	0.012	0.0048	0.074	18.0	11.0	36.0	30.0	207.0	0.5	0.5	0.5	17.0
052606-11					7.7	20.0	64.0	24.0	95.0	BDL	2.3	0.8	25.0
052606-9	5.12	0.14	0.006	0.094	40.0	21.0	35.0	89.0	131.0	0.2	2.1	0.3	64.0
052606-5	3.01	0.018	0.016	0.016	27.0	93.0	4921.0	BDL	24.0	3.1	6.6	5.8	1223.0
032206-7	2.94	0.016	0.007	0.052	18.0	35.0	75.0	31.0	392.0	0.6	1.1	1.4	49.0
032206-5	3.07	0.045	0.0075	0.048	11.0	16.0	110.0	26.0	115.0	1.5	1.8	1.0	24.0
010906-1	BDL	0.038	0.034	0.048	73.4	48.8	8.4	3.1	2.5	0.2	0.7	0.2	36.2
050506-26	BDL	0.063	0.022	0.076	111.1	59.7	13.7	3.4	1.9	0.5	0.2	0.2	36.4

Table 7. Selected composition of fluid inclusions based on LA-ICP-MS

Sample:	Wt % NaCl eq:	Na (23)	Mg (25)	K (39)	Ca (40)	Ti (49)	V (51)	Fe (56)	Co (59)	Ni (62)	Cu (63)	Zn (66)	As (75)
HLS-1D-A2-7.txt	1.70	178	221.7	430	1491	140	-	1358	-	-	2826	397	-
HLS-1D-A2-20.txt	1.70	842	62.3	839	756	204	14.34	502	-	64	1105	202	-
050906-5-FI1.txt	1.40	684	-	4451	68	-	-	-	-	-	1043	487	-
050906-5-FI3.txt	1.40	4277	-	665	304	-	-	-	-	-	-	-	-
050906-5-FI1.txt	1.40	684	-	4451	68	-	-	-	-	-	1043	487	-
050906-5-FI12.txt	1.40	343	25.6	6105	448	-	-	-	-	11	17	15	-
050906-5-FI12.txt	1.40	343	25.8	6104	449	-	-	-	-	11	17	15	-
050906-5-FI12.txt	1.40	328	42.9	6048	461	-	-	-	-	-	18	9	-
050906-5-FI13.txt	1.40	236	65.4	1450	205	26	-	914	-	-	1734	1578	-
050906-5-FI18.txt	1.40	1705	281.7	1538	864	-	-	293	-	-	412	532	-
050906-5-FI20.txt	1.40	915	87.3	1818	1132	-	-	105	-	-	1206	588	-
050906-5-FI21.txt	1.40	437	23.3	614	80	-	-	29	-	-	4807	471	-
050906-5-FI24.txt	1.40	735	635.2	1038	727	35	-	999	-	-	560	593	-
050906-5-FI27.txt	1.40	4736	-	696	70	-	-	-	-	-	-	-	-
050906-5-FI29.txt	1.40	2000	-	2081	-	-	-	-	-	-	752	431	-
050906-5-FI29.txt	1.40	4910	-	272	-	-	-	-	-	-	-	-	-
050906-5-FI31.txt	1.40	1092	967.0	1014	369	-	-	22	-	-	69	1861	-
050906-5-FI31.txt	1.40	3783	-	881	-	-	-	-	-	-	-	-	182
052106-3-FI4.txt	2.10	1166	-	5593	1033	-	-	496	-	-	457	-	-
052106-3-FI6.txt	2.10	1365	-	944	1172	-	-	1688	-	-	2000	315	-
052106-3-FI7.txt	2.10	1309	245.5	646	3843	-	-	537	-	-	672	715	-
052106-3-FI8.txt	2.10	2288	-	382	3812	-	-	1186	-	-	69	63	-
052106-3-FI8.txt	2.10	471	-	541	2686	-	-	703	-	-	67	3965	-
052106-3-FI8.txt	2.10	622	175.2	5605	2158	-	-	482	-	-	84	43	-
052106-3-FI10.txt	2.10	1666	-	5139	1677	-	-	134	-	-	122	441	-
052106-3-FI10.txt	2.10	2008	-	3426	2388	-	-	502	-	-	294	142	-
052106-3-FI11.txt	2.10	4304	-	4254	-	-	-	-	-	-	-	183	-
052106-3-FI12.txt	2.10	393	-	3784	2352	-	-	1122	-	-	259	440	-
052106-3-FI12.txt	2.10	415	204.7	7108	1673	-	-	101	-	-	70	89	-
052106-3-FI13.txt	2.10	793	96.9	7665	1196	-	-	73	-	-	35	50	-
052106-3-FI14.txt	2.10	773	-	6794	854	-	-	436	-	-	285	299	-
052106-3-FI15.txt	2.10	868	123.2	7246	1304	-	-	37	-	-	84	76	-
052106-3-FI16.txt	2.10	570	132.4	7096	1584	-	-	74	-	-	83	211	-
052106-3-FI16.txt	2.10	634	75.8	7610	1074	-	-	19	-	-	135	422	-
042706-7a-FI2.txt	1.60	1080	-	5953	409	-	-	-	-	-	-	-	-
042706-7a-FI12.txt	1.60	1740	247.6	1264	687	-	-	684	-	-	1440	255	-
042706-7a-FI13.txt	1.60	537	262.5	735	704	-	-	459	-	-	3270	617	-
042706-7a-FI13.txt	1.60	1189	125.1	1407	311	282	-	112	-	-	210	2511	-
042706-7a-FI14.txt	1.60	3557	-	-	350	-	-	172	-	-	170	1486	-
052406-3-FI2.txt	0.90	-	-	-	-	952	-	ND	1326	-	467	ND	-
052406-3-FI2.txt	0.90	-	-	-	-	783	-	ND	936	-	245	ND	-
052406-3-FI2.txt	0.90	-	-	-	-	751	-	ND	963	-	1102	ND	-
052406-3-FI9.txt	0.90	56	7.7	91	9	76	-	ND	118	-	3597	ND	-
052406-3-FI9.txt	0.90	-	-	-	-	576	-	ND	942	-	1723	ND	-
052406-3-FI3.txt	0.90	733	31.0	1242	108	-	0.69	516	67	36	503	100	-
052406-3-FI11.txt	0.90	971	6.9	242	8	41	-	2375	51	-	-	100	-
052406-3-2F-3.txt	0.90	1756	-	420	24	225	-	ND	257	-	814	ND	-
052406-3-2F-5.txt	0.90	951	-	228	15	359	-	ND	489	-	346	ND	-
052406-3-2F-5.txt	0.90	1810	-	492	30	258	-	ND	373	-	567	ND	-
052406-3-FI10.txt	0.90	-	-	-	-	19	-	ND	-	-	51	ND	-
052506-16-FI2.txt	0.20	482	-	213	-	-	-	-	-	-	-	-	-
052506-16-FI6.txt	0.20	290	-	451	-	11	-	11	-	-	20	-	-
052506-16-FI7.txt	0.20	449	-	-	-	24	-	-	-	-	-	-	-
052506-16-FI8.txt	0.20	105	-	476	20	-	-	152	-	-	29	-	-
052506-16-FI8.txt	0.20	37	17.5	286	41	-	-	273	-	-	112	15	-
052506-16-FI8.txt	0.20	90	-	435	54	-	-	100	-	-	43	11	-
052506-16-FI9.txt	0.20	575	-	-	-	-	-	-	-	-	-	-	-
052506-16-FI1.txt	0.20	589	-	-	-	-	-	-	-	-	-	-	-
060106-10-3.txt	0.20	79	-	548	102	-	-	17	-	-	-	-	-
060106-10-4.txt	0.20	124	35.3	531	71	-	-	7	-	-	-	3	-
060106-10-5.txt	0.20	43	28.9	44	67	-	-	295	-	-	220	27	-
060106-10-6.txt	0.20	26	-	53	26	-	-	14	-	571	45	54	-
060106-10-6.txt	0.20	82	-	146	87	-	-	46	-	72	153	159	-
060106-10-9.txt	0.20	397	-	123	79	-	-	23	-	-	9	71	-

Table 7. Selected composition of fluid inclusions based on LA-ICP-MS (Continued).

Sample:	Rb (85)	Sr (88)	Zr (90)	Mo (98)	Ag (107)	Ag (109)	Sn (120)	Sb (121)	Ba (138)	Hf (178)	W (182)	Au (197)
HLS-1D-A2-7.txt	-	10.77	8.27	-	-	ND	185.85	-	9.69	-	-	-
HLS-1D-A2-20.txt	-	2.81	1.62	20	-	ND	5.26	-	10.26	-	20.90	3.02
050906-5-FI1.txt	-	1.08	-	-	-	ND	-	-	-	-	-	-
050906-5-FI3.txt	-	33.97	-	-	-	ND	-	225	10.83	-	-	-
050906-5-FI1.txt	-	1.08	-	-	-	ND	-	-	-	-	-	-
050906-5-FI12.txt	4.06	0.30	-	-	-	ND	-	-	0.09	-	-	-
050906-5-FI12.txt	4.05	0.31	-	-	-	ND	-	-	0.09	-	-	-
050906-5-FI12.txt	4.70	0.40	-	-	-	ND	-	-	-	-	-	-
050906-5-FI13.txt	7.19	5.56	0.95	-	-	ND	84.49	19	5.55	-	2.81	4.75
050906-5-FI18.txt	-	3.02	-	-	-	ND	-	-	3.59	-	-	-
050906-5-FI20.txt	-	7.09	4.09	-	-	ND	11.74	23	4.97	-	0.95	-
050906-5-FI21.txt	-	4.19	1.41	-	-	ND	-	6	1.33	-	-	-
050906-5-FI24.txt	-	4.82	2.24	-	-	ND	61.21	29	3.64	-	3.38	3.68
050906-5-FI27.txt	-	-	-	-	-	ND	-	52	2.49	-	-	-
050906-5-FI29.txt	-	17.01	-	-	-	ND	-	128	11.40	14.95	-	-
050906-5-FI29.txt	-	-	-	-	-	ND	-	85	1.40	-	-	-
050906-5-FI31.txt	-	5.00	3.01	-	-	ND	-	75	0.92	-	-	-
050906-5-FI31.txt	-	6.33	-	-	-	ND	-	398	2.25	-	-	-
052106-3-FI4.txt	-	127.39	-	-	-	ND	117.00	-	55.04	-	10.35	19.08
052106-3-FI6.txt	-	16.90	-	-	-	ND	440.78	-	26.98	-	-	19.56
052106-3-FI7.txt	-	34.14	-	-	-	ND	-	-	12.60	-	-	-
052106-3-FI8.txt	-	9.99	-	-	-	ND	-	22	16.51	-	2.20	-
052106-3-FI8.txt	-	11.86	-	-	-	ND	-	37	7.15	3.88	-	-
052106-3-FI8.txt	16.31	27.52	-	-	-	ND	20.66	40	84.37	-	-	-
052106-3-FI10.txt	-	2.89	-	-	-	ND	20.82	-	2.69	-	-	-
052106-3-FI10.txt	-	25.02	7.28	-	-	ND	70.18	-	10.48	-	-	-
052106-3-FI11.txt	-	-	-	-	-	ND	-	-	9.99	-	-	-
052106-3-FI12.txt	-	18.82	-	-	-	ND	144.47	-	14.13	-	-	-
052106-3-FI12.txt	-	2.11	3.51	-	-	ND	-	-	2.63	-	-	-
052106-3-FI13.txt	8.17	1.50	-	-	-	ND	12.65	4	0.68	0.41	-	-
052106-3-FI14.txt	-	57.20	3.92	-	-	ND	42.22	122	53.88	-	-	-
052106-3-FI15.txt	-	3.36	-	-	-	ND	9.82	49	1.42	-	-	-
052106-3-FI16.txt	-	2.15	1.83	-	5	ND	9.33	-	-	-	-	-
052106-3-FI16.txt	6.04	1.96	4.70	-	-	ND	7.01	12	3.05	-	-	-
042706-7a-FI2.txt	-	3.00	-	-	-	-	-	-	2.28	-	-	-
042706-7a-FI12.txt	-	6.08	-	-	-	-	88.85	184	5.96	-	6.27	-
042706-7a-FI13.txt	-	14.86	-	-	-	-	119.72	44	11.21	-	5.32	-
042706-7a-FI13.txt	-	15.61	-	-	-	-	58.86	96	21.66	-	1.93	-
042706-7a-FI14.txt	-	8.42	-	-	-	-	-	106	-	-	-	-
052406-3-FI2.txt	-	-	-	-	574	ND	-	-	-	-	-	2.18
052406-3-FI2.txt	-	-	-	-	2024	ND	-	-	-	-	-	139.34
052406-3-FI2.txt	11.63	-	-	-	512	ND	-	-	-	-	-	1.55
052406-3-FI9.txt	-	0.10	-	-	35	ND	1.99	-	0.49	0.18	-	0.44
052406-3-FI9.txt	-	-	-	-	473	ND	-	-	-	-	-	6.15
052406-3-FI3.txt	-	0.40	1.59	-	388	ND	10.54	2	1.11	-	-	-
052406-3-FI11.txt	2.65	3.81	-	-	-	ND	-	4	-	-	-	0.07
052406-3-2F-3.txt	4.15	1.58	-	-	36	40	1.10	-	-	-	-	-
052406-3-2F-5.txt	2.60	1.07	0.25	-	19	16	-	-	0.13	0.45	-	-
052406-3-2F-5.txt	5.83	1.31	-	-	25	24	-	-	-	-	-	-
052406-3-FI10.txt	-	-	-	-	168		-	144	-	-	-	0.38
052506-16-FI2.txt	-	-	-	-	-	ND	-	23	0.42	-	-	-
052506-16-FI6.txt	-	-	-	-	-	ND	2.20	10	0.18	-	-	-
052506-16-FI7.txt	-	-	-	-	-	ND	-	138	1.00	-	-	-
052506-16-FI8.txt	-	1.21	-	-	-	ND	2.45	-	0.53	-	-	-
052506-16-FI8.txt	-	1.88	0.61	-	1	ND	10.12	6	1.91	-	0.76	0.52
052506-16-FI8.txt	-	4.66	-	-	-	ND	3.29	16	2.36	-	-	-
052506-16-FI9.txt	-	1.97	-	-	-	ND	-	17	-	-	-	-
052506-16-FI1.txt	-	-	-	-	-	ND	-	18	1.41	-	-	-
060106-10-3.txt	-	12.91	-	-	1	ND	-	47	6.59	-	-	-
060106-10-4.txt	0.95	7.40	0.19	-	15	ND	-	22	4.58	-	-	-
060106-10-5.txt	-	1.31	1.04	-	7	ND	12.66	-	1.21	-	-	-
060106-10-6.txt	-	1.35	-	-	-	ND	2.81	14	0.62	-	-	-
060106-10-6.txt	-	4.97	-	-	-	ND	8.69	49	1.99	-	-	-
060106-10-9.txt	-	1.02	-	-	2	ND	-	14	0.48	-	-	-

Table 7. Selected composition of fluid inclusions based on LA-ICP-MS (continued).

Sample:	Tl (205)	Pb (208)	Th (232)	U (238)
HLS-1D-A2-7.txt	-	110	0.66	-
HLS-1D-A2-20.txt	-	4658	0.65	1.20
050906-5-FI1.txt	-	107	-	-
050906-5-FI3.txt	-	-	-	-
050906-5-FI1.txt	-	107	-	-
050906-5-FI12.txt	-	1	-	0.01
050906-5-FI12.txt	-	1	-	0.01
050906-5-FI12.txt	-	1	-	0.00
050906-5-FI13.txt	-	257	-	0.27
050906-5-FI18.txt	-	209	-	-
050906-5-FI20.txt	-	428	-	3.90
050906-5-FI21.txt	-	55	-	-
050906-5-FI24.txt	-	437	-	-
050906-5-FI27.txt	-	-	-	-
050906-5-FI29.txt	-	151	-	-
050906-5-FI29.txt	-	4	-	-
050906-5-FI31.txt	-	61	-	1.74
050906-5-FI31.txt	-	-	-	-
052106-3-FI4.txt	-	70	-	3.80
052106-3-FI6.txt	-	165	-	-
052106-3-FI7.txt	-	142	-	9.62
052106-3-FI8.txt	-	42	-	-
052106-3-FI8.txt	-	35	-	-
052106-3-FI8.txt	-	27	-	6.80
052106-3-FI10.txt	-	24	1.67	1.55
052106-3-FI10.txt	-	33	-	-
052106-3-FI11.txt	-	-	-	-
052106-3-FI12.txt	-	49	1.36	1.95
052106-3-FI12.txt	-	7	-	-
052106-3-FI13.txt	-	13	-	0.18
052106-3-FI14.txt	-	42	-	-
052106-3-FI15.txt	-	4	-	-
052106-3-FI16.txt	-	11	-	-
052106-3-FI16.txt	-	3	-	-
042706-7a-FI2.txt	-	-	-	-
042706-7a-FI12.txt	-	53	-	-
042706-7a-FI13.txt	-	96	-	-
042706-7a-FI13.txt	-	832	-	-
042706-7a-FI14.txt	-	15	-	-
052406-3-FI2.txt	-	139	-	-
052406-3-FI2.txt	-	41	-	-
052406-3-FI2.txt	-	309	-	-
052406-3-FI9.txt	-	143	-	-
052406-3-FI9.txt	-	38	-	-
052406-3-FI3.txt	-	922	-	-
052406-3-FI11.txt	-	-	-	-
052406-3-2F-3.txt	-	122	-	-
052406-3-2F-5.txt	-	1921	-	0.38
052406-3-2F-5.txt	-	23	-	0.17
052406-3-FI10.txt	1.39	927386	-	-
052506-16-FI2.txt	-	-	-	-
052506-16-FI6.txt	-	-	-	-
052506-16-FI7.txt	-	-	-	-
052506-16-FI8.txt	-	1	-	-
052506-16-FI8.txt	-	3	-	-
052506-16-FI8.txt	-	1	-	-
052506-16-FI9.txt	-	-	-	-
052506-16-FI1.txt	-	-	-	-
060106-10-3.txt	-	-	-	-
060106-10-4.txt	-	-	-	-
060106-10-5.txt	-	4	-	0.23
060106-10-6.txt	-	1	-	-
060106-10-6.txt	-	2	-	-
060106-10-9.txt	-	-	-	-